



Copyright Undertaking

This thesis is protected by copyright, with all rights reserved.

By reading and using the thesis, the reader understands and agrees to the following terms:

1. The reader will abide by the rules and legal ordinances governing copyright regarding the use of the thesis.
2. The reader will use the thesis for the purpose of research or private study only and not for distribution or further reproduction or any other purpose.
3. The reader agrees to indemnify and hold the University harmless from and against any loss, damage, cost, liability or expenses arising from copyright infringement or unauthorized usage.

IMPORTANT

If you have reasons to believe that any materials in this thesis are deemed not suitable to be distributed in this form, or a copyright owner having difficulty with the material being included in our database, please contact lbsys@polyu.edu.hk providing details. The Library will look into your claim and consider taking remedial action upon receipt of the written requests.

THE HONG KONG POLYTECHNIC UNIVERSITY

DEPARTMENT OF APPLIED PHYSICS

**Study of Transport Properties at
LaAlO₃/SrTiO₃ Interface and Its
Application in Polar Molecule Sensor**

Au Kit

A thesis submitted in partial fulfilment of the requirements for
the degree of Master of Philosophy

JUNE 2012

Certificate of Originality

I hereby declare that this thesis is my own work and that, to the best of my knowledge and belief, it reproduces no material previously published or written nor material which has been accepted for the award of any other degree or diploma, except where due acknowledgement has been made in the text.

(Signature)

Au Kit (Name of candidate)



Abstract

Two-dimensional electron gas (2DEG) at oxide interface is a very interesting system that has been extensively studied in recent years. In this system, a 2DEG with high mobility ($\sim 10^3 \text{cm}^2 \text{V}^{-1} \text{s}^{-1}$ at 2 K temperature) is formed at the heterointerface between two band insulating materials LaAlO_3 (LAO) and SrTiO_3 (STO). This phenomenon has been explained by the model of electronic reconstruction due to the accumulation of polar discontinuity between the LaO and AlO_2 layers. Based on the model of electronic reconstruction and reported fabrication of field-effect transistor (FET) by 2DEG in oxide, the electric transport properties of the 2DEG should be able to be modulated by an external electric field or some polar molecules. In my thesis work, the application of the 2DEG as a polar molecule sensor has been demonstrated.

The oxide interfacial 2DEG was achieved by depositing LAO thin film on TiO_2 terminated STO substrate by Laser-MBE. Transmission electron microscopy (TEM) and atomic force microscopy (AFM) were used to characterize the structure of the LAO/STO interface. The electric transport properties of the heterointerface, including mobility, charge density and conductivity, were measured at temperatures from 2.5 to 300K.

When a droplet of water is added to the exposed LAO interface and fully covers the conducting channel, the I-V characteristic of the heterointerface changes to a typical FET type, but the rectify direction is different from the typical Schottky junction. An



THE HONG KONG POLYTECHNIC UNIVERSITY

explanation to this phenomenon is proposed based on the fact that the polar of liquid molecules should affect the polarization field inside the LAO film; while this effect may change the conducting behavior of the heterointerface from metallic to semiconducting, and therefore, a Schottky junction may be formed between the 2DEG and the affect area. It is also interesting to find that an amorphous STO layer on top of LAO surface results in the same kind of current saturation as that affected by polar liquid, suggesting that the a-STO on LAO also changes the transport properties of the underlying 2DEG.

These results not only promise the interest for understanding the oxide interfacial 2DEG, but also its potential applications in all-oxide device, thus may open new routes to complex oxide physics and ultimately for the design of devices in oxide electronics.



Scholarly Activity

Journal Papers

1. K. Au, D. F. Li, N. Y. Chan and J. Y. Dai, "Polar Liquid Molecule Induced Transport Property Modulation at LaAlO₃/SrTiO₃ Heterointerface", *Advanced Materials* 24 (19), 2598-2602 (2012).
2. Y. Chen, J. Y. Dai, K. Au, K. H. Lam, Y. B. Qin and H. X. Yang, "Temperature-dependent piezoelectric and dielectric properties of charge-ordered Lu₂Fe_{2.1}Mn_{0.9}O₇.", *Mater. Lett.* 68, 54-56 (2012).
3. X. S. Gao, J. M. Liu, K. Au, and J. Y. Dai, "Nanoscale ferroelectric tunnel junctions based on ultrathin BaTiO₃ film and Ag nanoelectrodes", *Appl. Phys. Lett.* 101, 142905 (2012).

Conference presentation

1. K. Au, X.S. Gao and J.Y. Dai "Study of BaTiO₃/Ag Nanostructured Ferroelectric Tunnel Junction", in 8th Cross-Strait Workshop on Nano Science & Technology (CNWNST) 2010
2. K. Au, N. Y. Chan and J.Y. Dai "Field effect of 2DEG at LaAlO₃/SrTiO₃ interface and its application as polar molecule sensor" in European Materials Research Society (EMRS) 2012 Spring meeting.



Acknowledgements

I would like to express my gratitude to my supervisor, J.Y. Dai for his guidance, support and assistance throughout my M.Phil study. He always gives me a large freedom on researches. I am so grateful for the latitude and care he gave me.

I would like to Special thanks should go to Prof. X.S. Gao. He is my mentor teaching on film deposition and the fundamental research skills patiently.

I sincerely thank D.F. Li, N.Y. Chan, Y.Y. Hau, Y. Chen and all my researches companions. They give me a lot of help that cannot be counted.

Finally, I would like to thank my parents for their endless love and support.



Table of contents

CERTIFICATE OF ORIGINALITY	II
ABSTRACT	III
SCHOLARLY ACTIVITY	V
ACKNOWLEDGEMENTS.....	VI
TABLE OF CONTENTS	VII
LIST OF FIGURES	XI
LIST OF TABLE	XVIII
CHAPTER 1 INTRODUCTION	19
1.1 BACKGROUND OF THESIS	19
1.2 WHAT IS TWO-DIMENSIONAL ELECTRON GAS (2DEG)?	20
1.3 TWO-DIMENSIONAL ELECTRON GAS (2DEG) IN $\text{LaAlO}_3/\text{SrTiO}_3$	22
1.4 TRANSPORTS PROPERTIES OF 2DEG AT $\text{LaAlO}_3/\text{SrTiO}_3$ INTERFACE	23
1.5 WHAT IS THE MECHANISM FORMING THE OXIDE 2DEG?.....	25
1.5.1 <i>Introduction to Perovskite Oxide</i>	25
1.5.2 <i>Electronic Reconstruction at $\text{LaAlO}_3/\text{SrTiO}_3$ Interface</i>	27



THE HONG KONG POLYTECHNIC UNIVERSITY

1.6 MOTIVATION OF THE THESIS WORK..... 31

1.7 OUTLINE OF THE THESIS 32

CHAPTER 2 FABRICATION AND CHARACTERIZATION METHODS.....34

2.1 SUBSTRATE TREATMENT..... 34

2.2 THIN FILM DEPOSITION 37

 2.2.1 *Introduction to Thin Film Deposition* 37

 2.2.2 *Laser-Molecular Beam Epitaxy*..... 38

 2.2.3 *Growth Modes of Thin Film*..... 39

2.3 STRUCTURAL CHARACTERIZATIONS 41

 2.3.1 *Epitaxial Growth Monitoring by RHEED*..... 41

 2.3.2 *Surface Topography Examined by Atomic Force Microscopy* 44

 2.3.3 *Film Structural Characterization by TEM*..... 46

2.4 SENSING DEVICE FABRICATION TECHNIQUES 47

 2.4.1 *Wire Bonding* 47

 2.4.2 *Parylene Coating*..... 48

 2.4.3 *Patterning of the LAO/STO heterointerface* 49

2.5 MEASUREMENT OF TRANSPORT PROPERTIES 51

 2.5.1 *Sheet Resistance Measurement*..... 51

 2.5.2 *Hall Measurement* 53

CHAPTER 3 CHARACTERIZATION OF LAALO₃/SRTIO₃

HETEROINTERFACE55

 3.1 INTRODUCTION..... 55



THE HONG KONG POLYTECHNIC UNIVERSITY

3.2 EXPERIMENTAL DETAILS 55

3.3 SURFACE QUALITY OF TREATED SUBSTRATES 57

 3.3.1 Treatment Process..... 57

 3.3.2 Topography of Substrate Surface..... 57

3.4 STRUCTURAL PROPERTIES OF LAO/STO HETEROSTRUCTURES..... 59

 3.4.1 Growth Process Monitored by RHEED 59

 3.4.2 Structure of thin films and interfaces 60

3.5 ELECTRICAL TRANSPORT PROPERTIES 61

3.6 WATER-PROOF SAMPLE PREPARATION..... 63

3.7 SUMMARY 66

CHAPTER 4 POLAR LIQUID MOLECULE INDUCED TRANSPORT

PROPERTY MODULATION AT LAALO₃/SRTIO₃ HETEROINTERFACE 67

4.1 INTRODUCTION..... 67

4.2 POLAR SENSING 68

4.3 SCHOTTKY DIODE-LIKE JUNCTION..... 71

4.4 SCHOTTKY JUNCTION COMPOSED OF METAL AND N-TYPE SEMI-CONDUCTOR JUNCTION 72

4.5 PROPOSED EXPLANATION OF THE BEHAVIOR 75

4.6 OTHER WORK..... 79

 4.6.1 Polar Liquid Molecule Induced Enhancement of Field Effect..... 79

 4.6.2 The 2DEG as DNA Sensor..... 82

4.7 SUMMARY 83

CHAPTER 5 FORMATION OF SCHOTTKY JUNCTION AT LAO/STO



THE HONG KONG POLYTECHNIC UNIVERSITY

INTERFACE WITH AMORPHOUS STO ON LAO84

5.1 INTRODUCTION 84

5.2 EXPERIMENTAL DETAIL 85

5.3 RESULT AND DISCUSSION 86

 5.3.1 Schottky Junction of between the 2DEG and a-STO..... 86

 5.3.2 Effect of Water on a-STO and 2DEG 87

 5.3.3 Temperature-Dependent I-V Characteristic of 2DEG/a-STO Schottky Junction..... 90

5.4 SUMMARY 94

CHAPTER 6 CONCLUSION AND PERSPECTIVES95



List of Figures

Figure 1-1 a) Schematic diagram of a MOSFET (adopted from Ref.[21]); b) illustration of band diagram between GaAs and Al doped GaAs showing the formation of 2DEG (adopted from Ref.[22]).....21

Figure 1-2 a) Cross-section of the gas sensor utilizing 2DEG (adopted from Ref.[24]), b) schematic representation of the terahertz detector combining 2DEG and CNT (adopted from Ref.[25])22

Figure 1-3 a) Sheet resistance of the 8-u.c. LAO/STO interface below 400 mK, the magnetic fields applied are perpendicular to the interface (adopted from Ref. [10]). b) Sheet resistance at 300 mK of an n-type SrTiO₃/LaAlO₃ conducting interface grown at 1.0×10^{-3} mbar. The arrows indicate the direction of the measurements (at a rate of 30 mT s^{-1}) (adopted from Ref. [4]).....25

Figure 1-4 Schematic sketch of the perovskite oxide ABO₃ structure. (a) One cubic unit cell of perovskite oxide consists of $8 \times 1/8$ A ions at the corners, a B ion at the center of the cube, and $4 \times 1/2$ O ions at the center of every faces; (b) ABO₃ structure can also be described as a stacking of AO and BO₂ atomic planes.....27

Figure 1-5 Schematic diagram of the resulting (LaO)⁺/(TiO₂)⁰ interface (a), and (AlO₂)⁻/(SrO)⁰ interface (b). (Adopted from Ref. [3]).....28

Figure 1-6 Schematic diagram of polar discontinuity. (Left) The structure of



THE HONG KONG POLYTECHNIC UNIVERSITY

unreconstructed interface; (Middle) electric potential diverging with LAO thickness due to the unreconstructed charge configuration; (Right) with the thickness of LAO above the threshold, the charge distribution was reconstructed and the potential divergence was removed. (Adopted from Ref. [43]).....30

Figure 1-7 Two application devices made by LAO/STO system realizing the memory behavior. a) The structure of FET device done by S. Thiel, with the thickness of LAO of 3 unit cells. b) The sheet resistance and the voltage of the back gate change with time (adopted from Ref.[7]). c) The structure of nanowires can be written and erased by utilizing C-AFM. d) The conductance between two electrodes measured as a function of the tip position across the wire (adopted from Ref.[11]).32

Figure 2-1 a) A single-terminated BO₂ surface with steps of about 0.4 nm high. The blue blocks correspond to the AO layer and the orange blocks to the BO₂ layer, with blue, orange, and white circles corresponding to A, B, and O ions, respectively. (Adopted from Ref.[45]) b) is BHF-treated SrTiO₃ substrates. The vertical profile was taken along the line indicated in the image. The BHF-treated substrate exhibits atomically flat terraces and 0.4 nm-high steps.....35

Figure 2-2 a) AFM image of the STO substrate after the surface treatment process, and b) the cross section along the line. (adopted at Ref.[46]).....36

Figure 2-3 a) A sketch of schematic diagram of L-MBE system and some deposition parameters (adopted from Ref. [57]) , and b) A photo of L-MBE system and



THE HONG KONG POLYTECHNIC UNIVERSITY

excimer laser in our laboratory.....39

Figure 2-4 Four different growth modes: (a) 2D layer-by-layer growth mode (Frank-Van der Merwe growth); (b) separated 3D islands mode (Volmer-Weber growth); (c) Stranski-Krastanov; (d) step-flow growth modes. (Adopted from [57]) 40

Figure 2-5 Schematic diagram of the study of film surfaces by RHEED. a) The sketch of the geometry of RHEED (Adopted from Ref.[57]), and b) RHEED pattern of SrTiO₃ substrate at ~720°C.....43

Figure 2-6 The surface models illustrating the growth of a single monolayer of film on a flat surface in layer by layer mode. The graph shows measured RHEED intensity during homoepitaxial growth of a single unit cell layer of SrTiO₃ (adopted from the website of RHEED company[65]).....44

Figure 2-7 a) Schematic diagram of working principle of AFM (adopted from Ref.[66]), and b) The SPM system in our laboratory.....46

Figure 2-8 A photo of PCB. The double sided tag was placed at the centre and it is the position for the sample.48

Figure 2-9 a) The chemical formula of parylene (Adopted from Ref.[69]), and b) is the equipment in our laboratory for parylene coating.49

Figure 2-10 The basic representation of the patterning process: a) Patterning of STO by photolithography; b) Growth of amorphous STO; c) lift off the photo-resist; d) deposition of single crystal LAO at the designed temperature50

Figure 2-11 (a) and (b) Two main types of the patterns used in my work.50

Figure 2-12 a) The electrode configuration of van der Pauw method(adopted from [71]).52



THE HONG KONG POLYTECHNIC UNIVERSITY

Figure 2-13 Schematic diagram of basic mechanism of Hall Effect (modified from [72])
.....54

Figure 3-1 AFM image of the treated STO substrate. The size of AFM images are 2x2 μm^2 : a) 40s etching by BHF; b) 60s etching by BHF; c) 90s etching by BHF; d) 120s etching by BHF; e) the flatten AFM image of (c); f) the surface profile of (e) showing vertical distance of the terrace of about 0.4 nm.58

Figure 3-2 RHEED pattern and the oscillation of the intensity: a) the oscillation of intensity of the RHEED pattern during the deposition of LAO on STO substrate; b) RHEED pattern of treated STO substrate prior to deposition at 750°C; c) RHEED pattern after 660s deposition of LAO which is the end of the deposition.60

Figure 3-3 (a) High-resolution TEM image of the LAO/STO interface, and (b) an enlarged image of (a). The number of unit-cell (9-10 u.c.) can be counted just as expected from RHEED intensity oscillation result.60

Figure 3-4 Temperature-dependent sheet resistance (a), and mobility (b), of the LAO/STO interface.62

Figure 3-5 I-V characteristic of the standard sample before and after parylene coating (total surface coated)64

Figure 3-6 Schematics diagram of the process of the water-proof sample: a) a piece of bare PCB; b) a piece of sample with the shape of long rod pasted onto the PCB; c) the connection between the copper on PCB and the conducting interface by bonding machine (ASM AB510); d) a blue tape was placed at the centre of the sample; e) the sample coated by the parylene; f) peel off the



THE HONG KONG POLYTECHNIC UNIVERSITY

blue tape to obtain the open window for testing.65

Figure 3-7 Photo of the standard water-proof sample.....66

Figure 4-1 (a) I -V curves of the LAO/STO interface with/without water droplet on top of LAO surface. The inset is a schematic diagram showing the sensor structure. (b) Schematic diagram illustrating water molecule alignment along the electrostatic field direction on the sample surface. The larger arrow indicates relatively larger polarization field, and the smaller arrow represents smaller polarization field in the LAO layer.70

Figure 4-2 (a) I -V curves of the LAO/STO interface with water on top of LAO surface but close to one end of electrode, and (b) schematic diagram illustrating water molecule alignment along the electrostatic field direction on the sample surface.....71

Figure 4-3 Energy-band diagrams of a metal with a higher work function in contact with a n-semiconductor: (a) before contacting, (b) after contacting in equilibrium, (c) under reverse bias and (d) under forward bias. (Modified from Ref. [89])73

Figure 4-4 I-V characteristic of the Schottky junction forming by the contact of metal and n-type semiconductor. The work function of metal is relatively larger. (Adopted from Ref. [90])74

Figure4-5 Energy-band diagrams of a metal with a lower work function contact to n-semiconductor: (a) before contacting, (b) after contacting in equilibrium, (c) and (d) are different direction of the bias.....75

Figure 4-6 Schematic band diagrams for the Schottky junctions formed along the



THE HONG KONG POLYTECHNIC UNIVERSITY

LAO/STO interface of the sample with water droplet in the center of the sample for, (a) zero bias voltage, and (b) non-zero bias voltage. (c-d) Schematic band diagrams when water droplet is close to one side electrode: (c) when $V_D > 0$, and (d) when $V_D < 0$77

Figure 4-7 a) I -V curves of the LAO/STO interface with/without PBS droplet on top of LAO surface and fully cover the conducting channel, while an external voltage is added by back gate. The I-V curve of the bare sample applied with back gate is shown as the reference; b) the photo of the sensor prototype; c) the pattern used for photolithography. Note: for this testing, there is no observable difference between water, PBS (water with K and Na ions) or PBS with DNA. So, only the data using PBS with DNA is used. ..81

Figure 4-8 I-V curves of sensors contact with (a) PBS with DNA, (b) PBS without DNA.83

Figure 5-1 Schematic diagram of the sample profile. For the connection between left side and centre, it is a typical connection of 2DEG. For the connection between right side and centre, a junction is formed between the 2DEG and the LAO layer.....86

Figure 5-2 (a) I -V curves of the connection between centre of sample and the right side, and (b) schematic diagram illustrating the connection of model. At the centre, the Aluminum wire is connected to the heterointerface by passing through the LAO thin film. For the Aluminum wire at the right side, it doesn't touch to the interface. This can be controlled by wire bonding force.87



Figure 5-3 (a) I-V curves of the sample under different connections at room temperature, and from (b) to (e) are schematic diagram illustrating the connection models. 89

Figure 5-4 I-V curves of the junction at different temperatures from 300K to 120K with an interval of 10K: a) the temperature-dependent I-V curves measured by centre to right; b) the temperature-dependent I-V curves measured by centre to left, (S6101 centre to right with a-STO); c) I-V curves at temperatures from 210K to 180K. The red arrow indicates the current maxima and the yellow arrow indicates the direction of loops. 93



LIST OF TABLE

Table 3-1 the parameters used for wire bonding of standard sample..... 61

Table3-2 Values of electric transport properties reported in different studies, where the data in this table are all taken at low temperature about 5 K (adopted from Ref.[76]). 63



Chapter 1 Introduction

1.1 Background of Thesis

In the revolutionary aspects in modern physics and device industries, perovskite oxides have provided foundation for concept of oxide-electronics and are continuously being explored for their potentials in novel applications. This is due to the broad spectrum of intrinsic functionalities of these oxides from dielectric property, piezoelectricity and ferroelectricity to superconductivity, magnetism as well as multiferroic behavior [1, 2]. These exceptional properties can also be used in electronic devices based on epitaxial heterojunctions. At such perovskite heterointerfaces, unexpected physical properties, which are absent in either of the individual bulk constituents, may arise [3]. One prominent example, as firstly reported by Ohtomo and Hwang in 2004 [3], is the discovery of a high-mobility ($\sim 10^4 \text{ cm}^2 \text{ V}^{-1} \text{ s}^{-1}$ at 4.2 K) two-dimensional electron gas (2DEG) with high carrier density ($10^{14} - 10^{17} \text{ cm}^{-2}$) [3-7] at heterointerfaces combining two band insulators LaAlO_3 (LAO) and SrTiO_3 (STO). After that, numerous prominent transport properties have been observed at such interface, for example, magnetic ordering [4, 8, 9], and superconductivity [10] can be found at low temperatures. Subsequently, Cen et al. showed that by applying a bias at conducting-tip as gate voltage in conductive atomic force microscopy (C-AFM) one can observe the local phase transition between insulating state and metallic state (which denote 0 and 1, respectively) [11-13]. Recently, there are many reports on the optical response on the



THE HONG KONG POLYTECHNIC UNIVERSITY

system as well [14, 15]. Upon this significant result, nanoelectronics fabrication platform could probably have the potential for widespread technological applications.

However, an almost empty area in this field of research is the application for such oxide interface 2DEG; while some preliminary phenomena toward sensor application have been reported. Most recently, H.Y. Huang's group has just reported the surface adsorption of polar liquid, such as water, induced large change (by factor of three) in the conductivity at the LAO/STO interfaces [16]. This conductivity change has been attributed to an increase of sheet carrier density of the 2DEG by more than $2 \times 10^{13} \text{ cm}^{-2}$, suggesting that the adsorbent has a great influence on the charge transfer from the film surface to the interface. These results also suggest that sensor application utilizing the surface-interface coupling induced conductivity modulation is possible. In this thesis work, I focus on applications utilizing the LAO/STO 2DEG in sensing devices (for example liquids) utilizing field-effect transistor structure.

1.2 What is Two-Dimensional Electron Gas (2DEG)?

A two-dimensional electron gas (2DEG) is a gas of electrons free to move in two dimensions, but tightly confined in the third. This tight confinement leads to quantized energy levels for motion in that direction. Thus the electrons appear to be a 2D sheet embedded in a 3D world. 2DEG is a very interesting system with some properties different from the traditional one in 3D world [17-19], for example, quantum



THE HONG KONG POLYTECHNIC UNIVERSITY

confinement effect or quantum hall effect [20]. It should be mentioned that quantum Hall Effect, which was first found in 2DEG, led to two Nobel Prizes in 1985 and 1998.

Practically, 2DEG was first found in MOSFETs of semiconductor system shown in Figure 1-1(a). When the transistor is in inversion mode, the electrons underneath the gate oxide are confined to the semiconductor-oxide interface, and occupy well defined energy levels. Nearly always, only the lowest energy level is occupied, and the electron is free to move parallel to the interface and the motion of the electron perpendicular to the interface is ignored. Therefore, it is regarded as quasi two-dimensional. The illustration is shown in Figure 1-1(b).

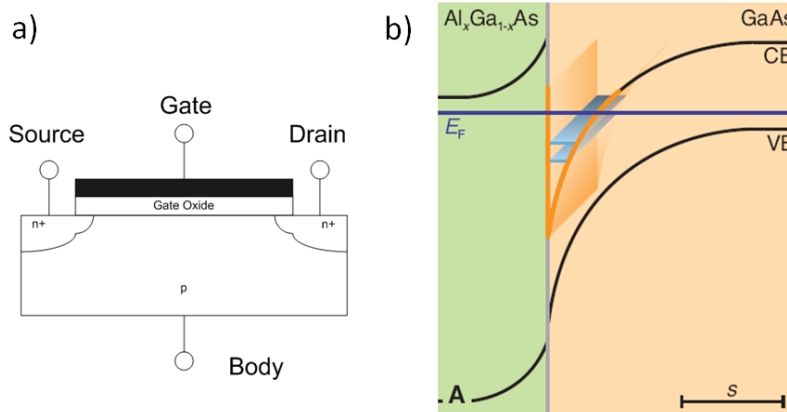


Figure 1-1 a) Schematic diagram of a MOSFET (adopted from Ref.[21]); b) illustration of band diagram between GaAs and Al doped GaAs showing the formation of 2DEG (adopted from Ref.[22])

2DEGs are also formed at semiconductor heterojunctions between different materials or materials with different doping levels, for example, GaAs/ $\text{Al}_x\text{Ga}_{1-x}\text{As}$ and GaN/ $\text{Al}_x\text{Ga}_{1-x}\text{N}$ are the well studied systems (Figure 1-2). In these systems, electrons



THE HONG KONG POLYTECHNIC UNIVERSITY

accumulate at the heterointerface well confined in a triangular quantum well due to this special band structure;, and mobility of the carriers of these 2DEGs can be very high. There are some applications of the 2DEG, for example, gas sensor, photodetector [23] and terahertz detector [24, 25].

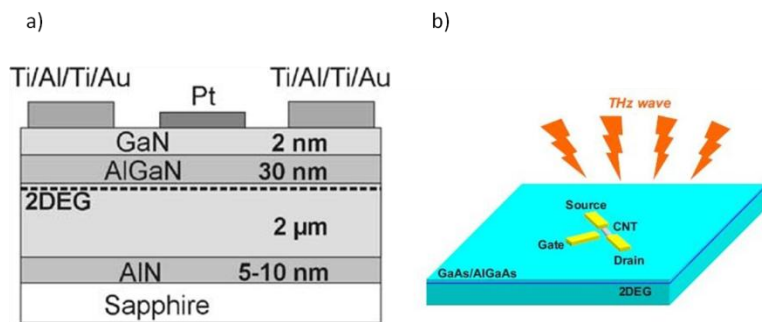


Figure 1-2 a) Cross-section of the gas sensor utilizing 2DEG (adopted from Ref.[24]), b) schematic representation of the terahertz detector combining 2DEG and CNT (adopted from Ref.[25])

1.3 Two-Dimensional Electron Gas (2DEG) in LaAlO₃/SrTiO₃

Not only in semiconductor interfaces, 2DEGs have also been discovered at oxide interfaces. One of the recent hot topics is the perovskite oxide LaAlO₃/SrTiO₃ (LAO/STO) heterointerface system reported by Ohtomo and Hwang in 2004 [3], where a conducting layer of two-dimensional electron gas (2DEG) is formed when these two large-band gap insulators join together. Since the first report, many interesting phenomena have been observed in this conducting heterointerface, including superconductivity [10] and indications of magnetism [4]. In addition, its interfacial electronic states can also be tuned by controlling external bias field [26]. It is worthy to notice that more physical properties have been observed, predicted and discussed in



THE HONG KONG POLYTECHNIC UNIVERSITY

both theoretical [27-30] and experimental [4, 10, 12, 26, 31-33] work, showing that the 2DEG formed at the interface of LAO/STO is similar to those formed at conventional semiconductor interfaces. However, there is still debate on the origin of the conductivity and high mobility of the system [6, 28, 33-36].

Compared to semiconductor heterostructure, oxide heterostructure and multi-layers are much more difficult to fabricate. The research in this field has been limited for many years, and until last two decades, the growth of oxide structure was well developed. Many new growth techniques and characterization methods made a large benefit to the fabrication. For example, high vacuum pulsed-laser deposition (PLD) and molecular-beam epitaxy (MBE) provide the possibility to grow high-quality oxide thin films; different substrate surface treatment methods give the ability of obtaining well-defined terminations of substrates; high-pressure reflection high-energy electron diffractions (RHEED) can monitor the growth of oxide thin film at high oxide pressure. As a result, fabrication of oxide epitaxial heterostructure can be achieved, and the precision of oxide heterostructure growth can be controlled in atomic scale.

1.4 Transports Properties of 2DEG at $\text{LaAlO}_3/\text{SrTiO}_3$ Interface

In 2006, Thiel *et al.* studied the relation between conductivity of 2DEG and the thickness of LAO layer [7]. It has been found that the conductivity was not related to the thickness of LAO; while it changed from insulating to metallic as long as the



THE HONG KONG POLYTECHNIC UNIVERSITY

thickness of LAO is thicker than 4 unit cells. This result reconciles the polar discontinuity model as the thickness of LAO layer has to be over a critical thickness so that the built-up potential within LAO is large enough to make electrons reconstructing as a conduction band at the interface. However, there is still an open question that the resulted carrier concentration at the interface is far lower than the expected value (assuming 0.5 electron per 2D unit cell was reconstructed.)

After that, other properties have also been reported. In 2007, Reyren *et al.* reported superconductivity in this system when temperature was under 200mK [10]. This transition into superconductivity was considered as Berezinskii-Kosterlitz-Thouless (BKT) transition from current voltage relation and temperature-dependent sheet resistance. Although a clear picture of this mechanism for the superconductivity at the interface cannot be obtained, the fact that the sheet carrier density is very high suggests that the 2DEG in the LAO/STO system is not caused by oxygen vacancies.

Later on, a phase diagram of electric field controlling effect to the ground state of LAO/STO interface, changing between superconducting and insulating, was reported [26]. Based on this finding, large and tunable spin-orbit interaction and negative magnetoresistance were also discovered [32, 37]. Recently, quantum capacitance and quantum oscillation properties [38] of this system were also reported [39, 40]. All of these reported transport properties contribute to the picture of this interesting system.

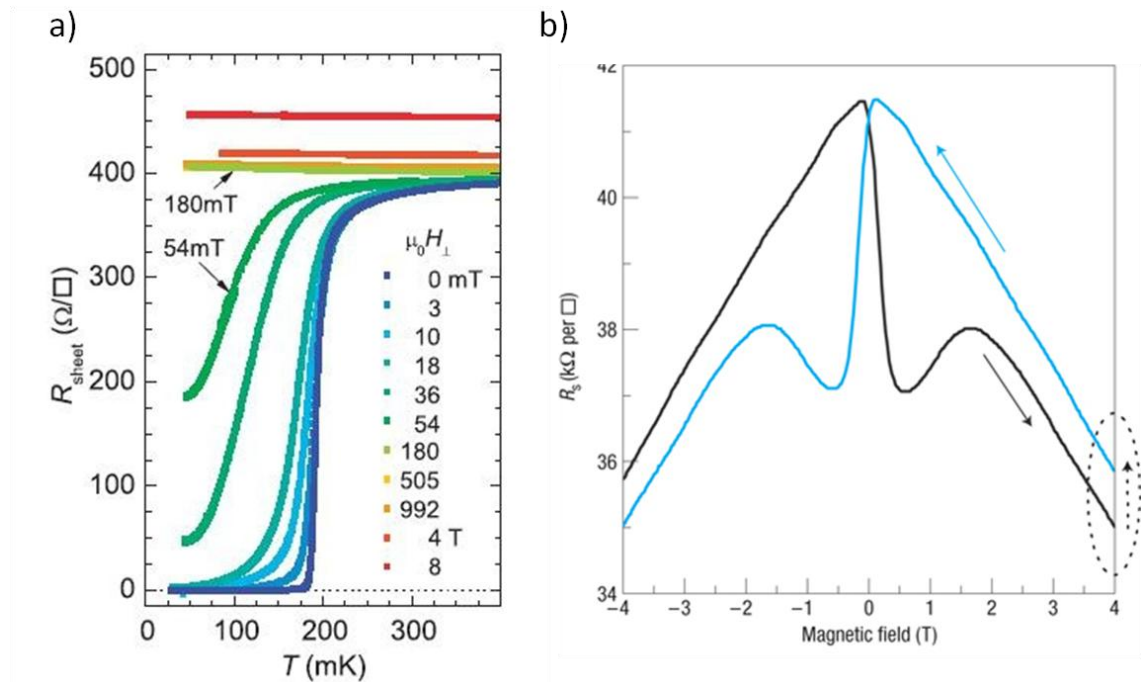


Figure 1-3 a) Sheet resistance of the 8-u.c. LAO/STO interface below 400 mK, the magnetic fields applied are perpendicular to the interface (adopted from Ref. [10]). b) Sheet resistance at 300 mK of an n-type SrTiO₃/LaAlO₃ conducting interface grown at 1.0×10^{-3} mbar. The arrows indicate the direction of the measurements (at a rate of 30 mT s^{-1}) (adopted from Ref. [4]).

1.5 What Is the Mechanism Forming the Oxide 2DEG?

1.5.1 Introduction to Perovskite Oxide

Since the oxide interfacial 2DEGs so far reported are only in the perovskite oxide interfaces, it is worthy to have a general introduction of perovskite oxide structure. The general formula of perovskite oxide is ABO_3 , where O is oxygen anion, A and B are a relatively larger and smaller cations, respectively. The schematic structure of perovskite



THE HONG KONG POLYTECHNIC UNIVERSITY

oxide was shown in Figure 1-4(a). All compound oxides with this chemical formula are in this family.

The crystal structures of the family can be changed in many different forms, including cubic, tetragonal, orthorhombic, rhombohedra and monoclinic depending on the temperature and chosen elements of A and B. Perovskite oxide also shows multiple properties, for example, insulating, semi-conducting, metallic, super-conducting, pyroelectric, piezoelectric, ferroelectric, ferromagnetic, and anti-ferromagnetic and multiferroic behavior[1, 2, 41] depending on the temperature and chosen elements of A and B. As there are many different elements can be chosen as A and B, the properties and behavior can be controlled depending on need. Therefore, perovskite oxide can be used in many different aspects and be included in many research. It is worthy to notice that the structure of perovskite oxide can also be considered as a sequence of alternating AO and BO₂ atomic layers along the (001) planes. The schematic model of perovskite oxide is shown in Figure 1-4(b).

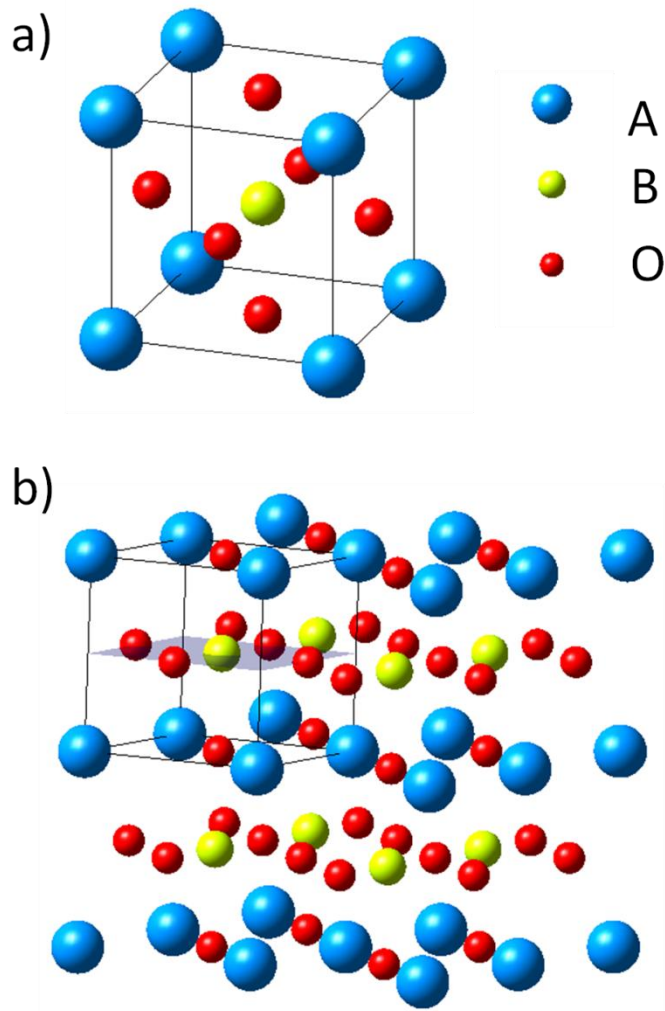


Figure 1-4 Schematic sketch of the perovskite oxide ABO_3 structure. (a) One cubic unit cell of perovskite oxide consists of $8 \times 1/8$ A ions at the corners, a B ion at the center of the cube, and $4 \times 1/2$ O ions at the center of every faces; (b) ABO_3 structure can also be described as a stacking of AO and BO_2 atomic planes.

1.5.2 Electronic Reconstruction at $LaAlO_3/SrTiO_3$ Interface

It is very surprising and interesting that a conducting interface is formed between LAO and STO, while both LAO and STO are originally insulating. The origin of this



THE HONG KONG POLYTECHNIC UNIVERSITY

conducting 2DEG is still under intensive debate theoretically and experimentally. The first explanation was proposed by Ohtomo and Hwang. In their paper [3], the fundamental mechanism was studied by preparing the sample with two types of different stacking. They grow LAO on top of STO substrate in [001] direction, along which perovskite oxide (ABO_3) can be considered as a sequence of alternating AO and BO_2 atomic layers. In this situation, two kinds of interfaces can be formed between LAO and STO, as shown in Figure 1-5.

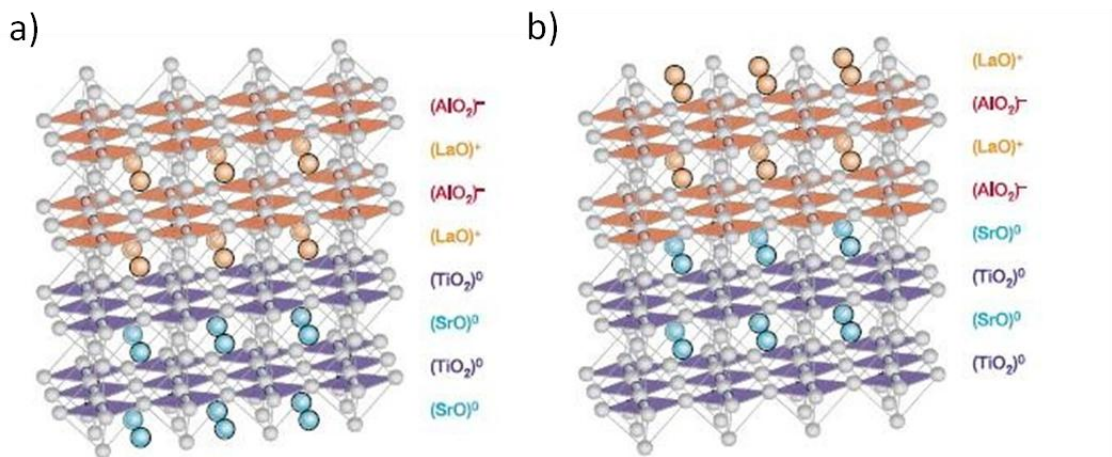


Figure 1-5 Schematic diagram of the resulting $(LaO)^+/(TiO_2)^0$ interface (a), and $(AlO_2)^-/(SrO)^0$ interface (b). (Adopted from Ref. [3])

When LAO is epitaxially grown on STO, a particular type of interface will be formed depending on the termination of STO substrate. In Figure 1-5(a), TiO_2/LaO interface is established on TiO_2 termination; while in Figure 1-5(b), SrO/AlO_2 interface is built on SrO termination. It is also shown in their paper [3] that the electric transport properties of these two kinds of interfaces are dramatically different. The TiO_2/LaO type of interface is highly conducting and behaves as metallic, while the SrO/AlO_2 type of interface is insulating.



Due to the different valence states of the cations, LAO can be considered as alternatively placed charged planes (LaO^+ and AlO_2^-); while STO is described as the sequence of charge-neutral planes (SrO^0 and TiO_2^0). Therefore, due to the sequence of charged plane, a potential was built within LAO layer, and a polar discontinuity is formed at the interface when LAO is grown on STO. Actually, this polar discontinuity has been named as “polar catastrophe”, which was first discussed in 1980s for the semiconductor heterostructures of Ge/GeAs [42].

For a semiconductor system, to avoid such polar catastrophe, the atoms at the interface would redistribute, named as atomic reconstruction. Actually, this kind of movement of atoms leads to interface roughness, whereas it is the only option to let the system stable. For the interface formed by complex oxides such as LAO/STO, some of the cations have mixed valences allowing for charge compensation by accommodating extra electrons in their bands. At the conducting TiO_2/LaO interface in LAO/STO heterojunctions, electrons can cross the interface and be accepted by interfacial Ti ions, leading to a n-type conducting interface. This causes Ti^{4+} ions to become Ti^{3+} , eliminating the divergence of the electrostatic potential within LAO layer (shown in Figure 1-6). Therefore, this new phenomenon was proposed to be electronic reconstruction.[3] [43]

THE HONG KONG POLYTECHNIC UNIVERSITY

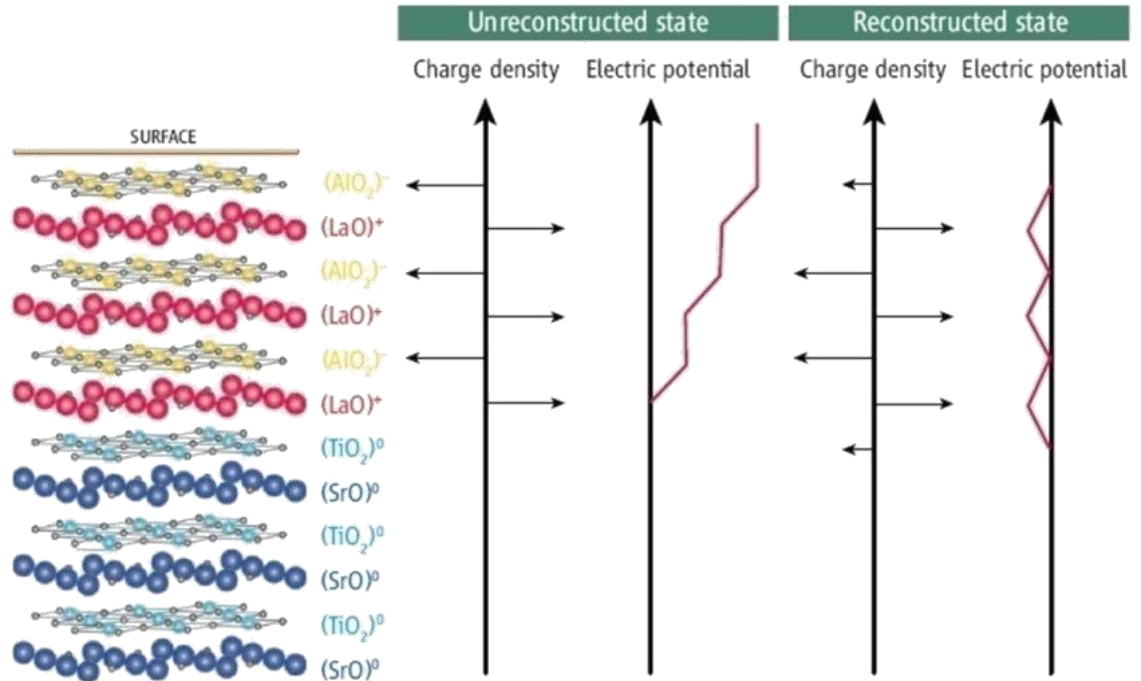


Figure 1-6 Schematic diagram of polar discontinuity. (Left) The structure of unreconstructed interface; (Middle) electric potential diverging with LAO thickness due to the unreconstructed charge configuration; (Right) with the thickness of LAO above the threshold, the charge distribution was reconstructed and the potential divergence was removed. (Adopted from Ref. [43])

The electronic reconstruction provides a good interpretation on the origin of the metallic interface between LAO and STO, however, it cannot be used to explain all the behaviors, such as why the SrO/AlO₂ interface is insulating. There are many possibilities proposed, for example, the conducting behavior may be caused by the oxygen vacancies in STO substrate, or by an ultrathin inter-diffusion layer. Nevertheless, the electronic reconstruction is still the most accepted model of this phenomenon; however, the entire story is still under ongoing debate.



1.6 Motivation of the Thesis Work

Since the first report on discovery of the two-dimensional electron gas at LaAlO₃/SrTiO₃ (LAO/STO) interface in 2004, there has been a great attraction to scientists to study the mechanism of forming 2DEG at this oxide interface. However, an almost empty area in this field of research is the application of such oxide interface 2DEG; though some preliminary phenomena toward sensor application have been reported, such as shown in Figure 1-7 [16]. Most recently, H.Y. Huang's group has just reported the surface adsorption of polar liquid, such as water, induced large change (by a factor of three) in the conductivity at the LAO/STO interface [16]. This conductivity change has been attributed to an increase of sheet carrier density of the 2DEG by more than $2 \times 10^{13} \text{ cm}^{-2}$, suggesting that the adsorbent has a great influence on the charge transfer from the film surface to the interface. These results also suggest that sensor application is possible by utilizing the surface-interface coupling induced conductivity modulation. In this thesis work, I focus on applications utilizing the oxide 2DEG in sensing devices, such as polar liquids utilizing field-effect transistor structure.



THE HONG KONG POLYTECHNIC UNIVERSITY

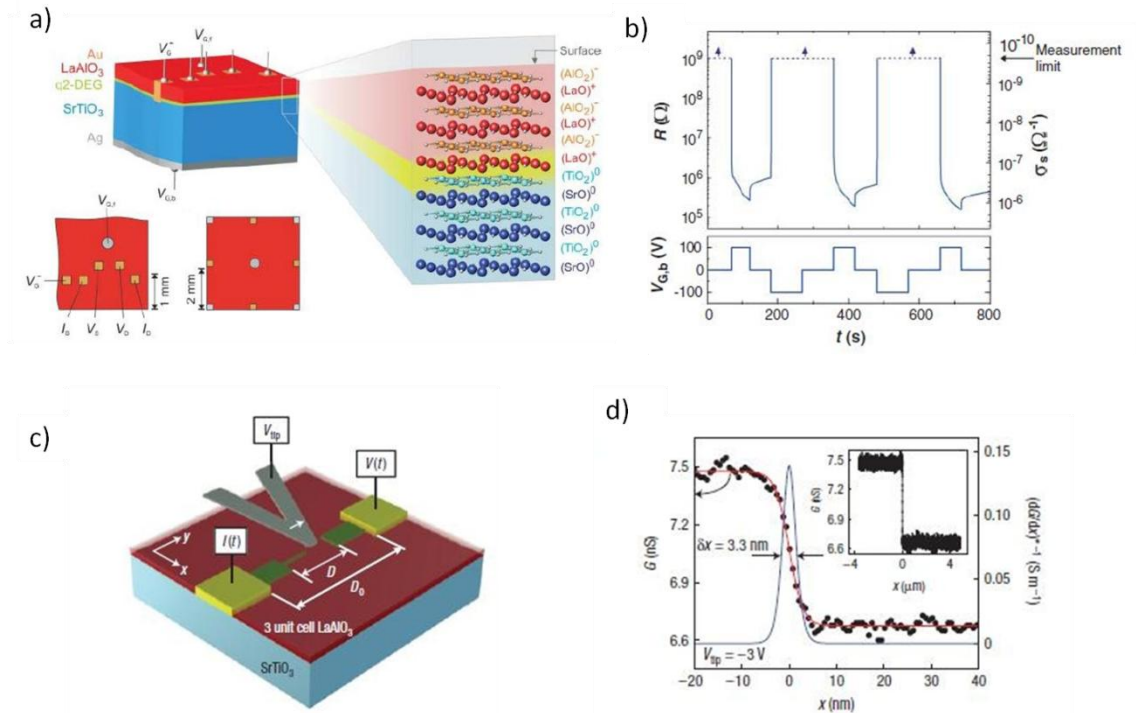


Figure 1-7 Two application devices made by LAO/STO system realizing the memory behavior. a) The structure of FET device done by S. Thiel, with the thickness of LAO of 3 unit cells. b) The sheet resistance and the voltage of the back gate change with time (adopted from Ref.[7]). c) The structure of nanowires can be written and erased by utilizing C-AFM. d) The conductance between two electrodes measured as a function of the tip position across the wire (adopted from Ref.[11]).

1.7 Outline of the Thesis

A brief literature review is given in Chapter 1, including “what is 2DEG” and the finding of 2DEG in LAO/STO system, the mechanism of forming 2DEG and the basic transport properties of it. Motivation of this thesis work is also introduced.

Chapter 2 gives a short introduction to those techniques that have been employed in this study including substrate treatment, deposition techniques, structural characterization



THE HONG KONG POLYTECHNIC UNIVERSITY

techniques, sensor preparation and transport measurement setups.

In Chapter 3, the characterizations of LAO/STO have been reported. This chapter mainly focuses on the characterizations and basic transport properties of samples used in the thesis. Experimental details including procedures and parameters are also introduced.

In Chapter 4, the phenomenon of polar liquid molecule induced transport property modulation at LAO/STO interface is reported. Also, some of the experiments based on this phenomenon are introduced in this chapter.

In order to understand more about the previous findings, in Chapter 5, a similar junction structure to the water affected 2DEG was formed by depositing amorphous STO on the LAO surface.

Chapter 6 gives the conclusions of this thesis and future perspectives in this field of research.



Chapter 2 Fabrication and Characterization Methods

2.1 Substrate Treatment

As reported by H.Y. Hwang in 2004 [3] and proved by many followed work that to form a TiO_2 terminated surface on STO is essential to form 2DEG at the LAO/STO interface. But in fact, study of surface treatment of perovskite oxide, including STO, has been carried out many years ago before the first report of LAO/STO 2DEG, since surface treated substrates with single termination is essential for a high-quality epitaxial and atomically flat thin film growth. The first effective surface treatment method of STO was published by Masashi Kawasaki in 1994 [44], in which a method using $\text{NH}_4\text{-HF}$ (called as buffed HF solution) to dissolve SrO and obtain Ti-terminated STO substrate is introduced. STO surface treatment is not only important for this work, but in general is also significant for other thin film growth studies.

As described in Chapter 1, STO is one type of perovskite which has two possible terminations including Ti-site and Sr-site. Usually, the surface of a normal STO substrate has a mixture of both two-site terminations. Considering the fact that TiO_2 is natural oxide and SrO is acidic oxide, by controlling the pH value of buffed HF solution, the BHF solution will mainly dissolve the Sr atom but react very slightly with Ti atom. Therefore, the top surface Sr layer in contact with the BHF solution will be etched out;



THE HONG KONG POLYTECHNIC UNIVERSITY

while the Ti ions on the removed Sr ions would also be lift-off. After such an etching process, a step-and-terrace structure will be formed, as shown in Figure 2-1. From the AFM image of the etched STO surface, a step height ~ 0.4 nm indicates that those steps are single unit-cell high corresponding to the lattice constant of STO ($a=3.905$).

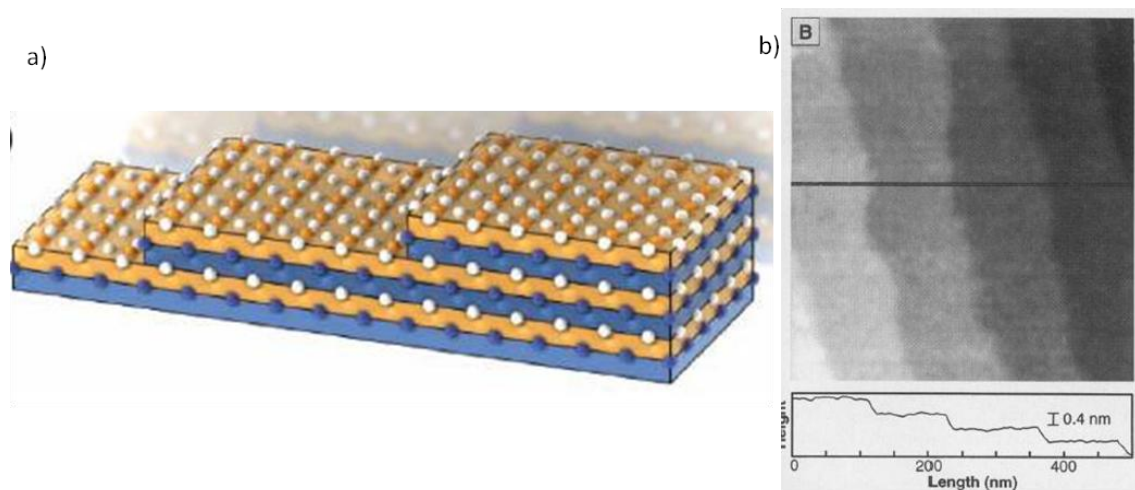


Figure 2-1 a) A single-terminated BO₂ surface with steps of about 0.4 nm high. The blue blocks correspond to the AO layer and the orange blocks to the BO₂ layer, with blue, orange, and white circles corresponding to A, B, and O ions, respectively. (Adopted from Ref.[45]) b) is BHF-treated SrTiO₃ substrates. The vertical profile was taken along the line indicated in the image. The BHF-treated substrate exhibits atomically flat terraces and 0.4 nm-high steps.

This surface treatment method is an effective way to obtain an atomic-flat STO substrate with Ti-site termination. However, during the etching process, ph value of the BHF solution has to be controlled very strictly; there will be many remnants on the surface if ph value of the BHF solution is too low; while conversely, there will be many holes formed if ph value of the BHF solution is too high. Therefore, it is difficult to control the etching process and reproduction of samples, and most of the time, there will



be a lot of holes and remnants on the surface.

Until 1998, Gertjan Koster found out a method to solve this problem where the etching quality highly depends on the ph value of BHF solution [46]. A step was added into the procedure where the substrate was soaked into de-ionized water before etching with BHF solution. The SrO at topmost layer will react with water forming Sr-hydroxide complex, which can be easily dissolved in acid, so that the etching process much favor to Sr than Ti ions. This method can reduce the reaction time and make the ph value of BHF less crucial, and therefore, can successfully reduce the hole and remnants formed on the surface and increase the reproducibility. It was also reported that an annealing process was added after BHF etching. During the annealing, the substrate was placed in 1atm oxygen pressure at temperature of 850°C to remove residuals and help recrystallization. Figure 2-2(a) shows an AFM image of the completely treated substrate.

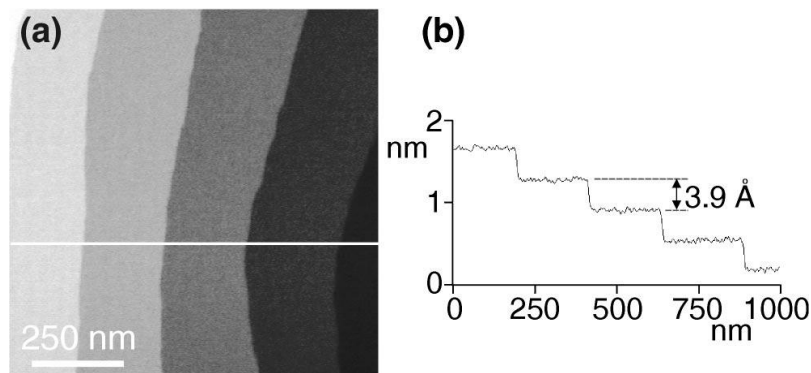


Figure 2-2 a) AFM image of the STO substrate after the surface treatment process, and b) the cross section along the line. (adopted at Ref.[46])



After these two main reports of substrate treatment methods, there are many ongoing researches on it. For example, a short re-etching was added to the final process [47, 48]. In some reports, instead of using BHF solution, HCLNO (HCL: HNO₃) was used to etch the substrate [49-51]. In this thesis work, the method proposed by Gertjan Koster was used.

2.2 Thin Film Deposition

2.2.1 Introduction to Thin Film Deposition

The physical vapor deposition (PVD) technique is one of the most effective ways to grow thin film especially for the ultra-thin film that allows investigation of properties of sample with strong strain or stress effects or properties at the heterointerface. PVD can be mainly divided into four categories, which are evaporation, sputtering, cathodic arc-deposition and pulsed-laser deposition (PLD).

Among these deposition methods, PLD is one of the most common techniques used for fabricating high-quality oxide, nitride, semiconductor and metal thin films (e.g. LAO, LSMO, Au, Pt, etc)[52-55]. PLD has a lot of advantages compared to other PVD techniques mentioned above, such as: (1) a lot of different materials of single element or compound can be used to grow thin films; (2) the growth rate can be easily and well controlled; (3) different ambient gases can be used to increase the variety of material



THE HONG KONG POLYTECHNIC UNIVERSITY

growth; and (4) the stoichiometry of the thin films can be preserved from the target materials, provided that the growth parameters are optimized. Of course, such technique also has its own drawbacks, for examples: (1) the small deposition area due to space distribution effect; (2) high cost because of the high vacuum system and the high power pulsed laser; and (3) low production. Those reasons limit its possibility to be utilized in industries, but it is very suitable for research aim using in laboratory.

Molecular Beam Epitaxy (MBE) is a very powerful technology with advantages such as: (1) the high-quality semiconducting material thin film can be grown because of its ultra-high vacuum chamber (most of the semiconducting elements are highly reactive with oxygen especially at high temperature); (2) the growth can be controlled in atomic-level with the help of reflection high-energy electron diffraction (RHEED) system; and (3) the stoichiometry of the grown thin films can be controlled during the growth process. But it also has some disadvantages, such as, hard to be controlled and low growing rate of thin film (typically less than 1000nm per hour).

2.2.2 Laser-Molecular Beam Epitaxy

In my work, laser-molecular beam epitaxy (L-MBE) was used to grow the LAO films with high quality epitaxial heterointerfaces. L-MBE is a powerful system combining the advantages of PLD and MBE [56]; L-MBE is similar to traditional PLD method, but equipped the ultra-high vacuum chamber using complex pumping system and RHEED



THE HONG KONG POLYTECHNIC UNIVERSITY

system to monitor the atomic level growth situation.

In PLD, a high energy pulsed laser is focused and used as the source ablating on the desired target material. A rapid congruent evaporation is induced by strong absorption of such a high energetic electromagnetic radiation creating plume. The plume passes through the vacuum and atoms are deposited on the substrate. Finally, the ablated material nucleates and grows into a thin film on the substrate surface. Of course the growth process can be monitored by RHEED system and the mechanism of it will be discussed later. A schematic diagram of the working principles of the L-MBE system used in our lab is shown in Figure 2-3

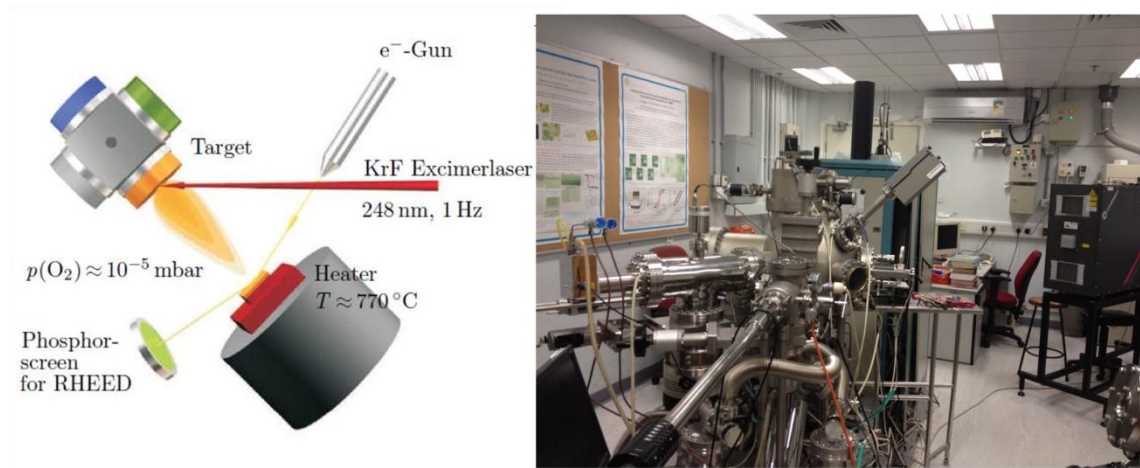


Figure 2-3 a) A sketch of schematic diagram of L-MBE system and some deposition parameters (adopted from Ref. [57]) , and b) A photo of L-MBE system and excimer laser in our laboratory.

2.2.3 Growth Modes of Thin Film

During the deposition process, as mentioned before, high energy pulse laser ablates



THE HONG KONG POLYTECHNIC UNIVERSITY

material from the target surface and atoms, ions, and molecules passing through the vacuum and finally reach the substrate surface, and be either elastically reflected out of or captured on the substrate surface. Those captured particles, called adatoms, will be subject to desorption, adsorption and diffusion on the surface and steps, and eventually nucleate and grow into a film. There are four different growth modes can be distinguished shown in Figure 2-4. They occur mainly depending on the free energies of the substrate surface (γ_s), film surface (γ_f), and film-substrate interface (γ_I). 2D layer-by-layer growth mode (Frank-Van der Merwe growth) occurs if the bonding between the film and substrate is strong, considering $\gamma_f + \gamma_I < \gamma_s$ [58]. However, if bonding between the substrate and the film is weak [59], separated 3D islands mode (Volmer-Weber growth) will grow and finally coalesce. In some cases, the lattice mismatch between the substrate and the film is too large to giving rise to biaxial strain, resulting in an elastic energy increasing with increased layer thickness, and therefore Stranski-Krastanov growth mode (Starting by complete monolayer growth but end up by appearance of islands) will appear [60]. For step-flow mode, it can be found if the diffusion time (relaxation time) of atoms on a terrace is very fast (relaxation time of the atoms growing on the surface is shorter than the laser rest time). In this growth mode, the adatoms move to the step edges and nucleation on a terrace is prevented, and therefore, no island growth will be observed.

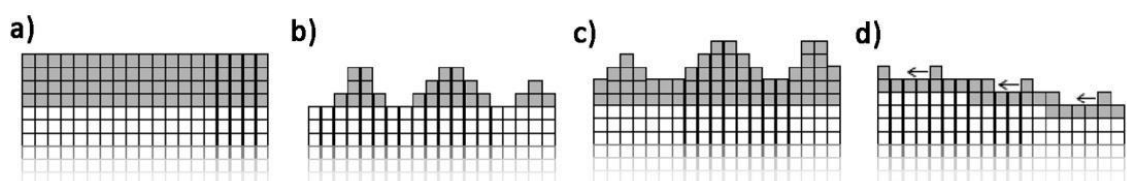


Figure 2-4 Four different growth modes: (a) 2D layer-by-layer growth mode (Frank-Van der



THE HONG KONG POLYTECHNIC UNIVERSITY

Merwe growth); (b) separated 3D islands mode (Volmer-Weber growth); (c) Stranski-Krastanov; (d) step-flow growth modes. (Adopted from [57])

As different growth modes may occur during a film growth, in order to fabricate high quality thin films, there are several parameters need to be considered and optimized. They are mainly: (1) Laser parameters including laser fluence (joule/cm^2), laser energy and the frequency of the pulsed-laser. These parameters mainly affect the film quality, the stoichiometry and the deposition flux of the grown thin film; (2) Surface temperature of the substrate, which has a large effect on the nucleation density; (3) The Surface of the substrate, including the miscut angle, the roughness and the termination site of the substrate; and (4) Background pressure, including the vacuum level, gas types of background, which is needed to ensure the stoichiometry transfer from the target to the film. [46, 61-63]

2.3 Structural Characterizations

2.3.1 Epitaxial Growth Monitoring by RHEED

Reflection high-energy electron diffraction (RHEED) is a technique used to characterize the surface of crystalline materials by utilizing the information from diffraction of electron by the surface of the substrate[64]. Also, RHEED are usually used to monitor the growth of the thin film by continuously providing the information of the surface of thin film.



THE HONG KONG POLYTECHNIC UNIVERSITY

Typically, A RHEED system is composed of an electron gun, a phosphor screen image detector (CCD camera) and, of course, a processor and software for analysis of the collected information. For the RHEED system used to monitor the growth of oxide thin film, it would also be composed by the double pumping system. The vacuum of the backside of the electron gun needs to be maintained at a very high level, whereas the front side of the electron gun was exposed to the main chamber. Usually, the vacuum of the main chamber is needed to maintain at a relatively low level (a higher oxygen pressure) for high-quality oxide thin film growth. With the complex double pumping system, RHEED system can be operated up to 15 Pa oxygen pressure and be more functional in oxide thin film fabrication. (This pressure was almost the highest pressure for operation of RHEED system, not only because of the needing of high vacuum of the back side of the electron gun, but also because of the mean free path of the electron in main chamber)

RHEED is a surface-sensitive system. The incidence angles of the electron beam cutting on the surface of the substrate is very low, therefore, the penetration depth of electron is very low. Experimentally, RHEED only senses a few top atomic layers of the surface, therefore, the sensing volume can be regarded as a two-dimensional layer. Therefore, a set of one-dimensional rods would be degenerated by the reciprocal lattice along the z direction perpendicular to the surface of the sample. The geometry of the electron beam, substrate and the phosphor screen is illustrated in Figure 2-5(a). When the reflected electron beam hit on the phosphor screen, the phosphor material would be



THE HONG KONG POLYTECHNIC UNIVERSITY

lighted and the information was recorded by the image detector shown in Figure 2-5(b).

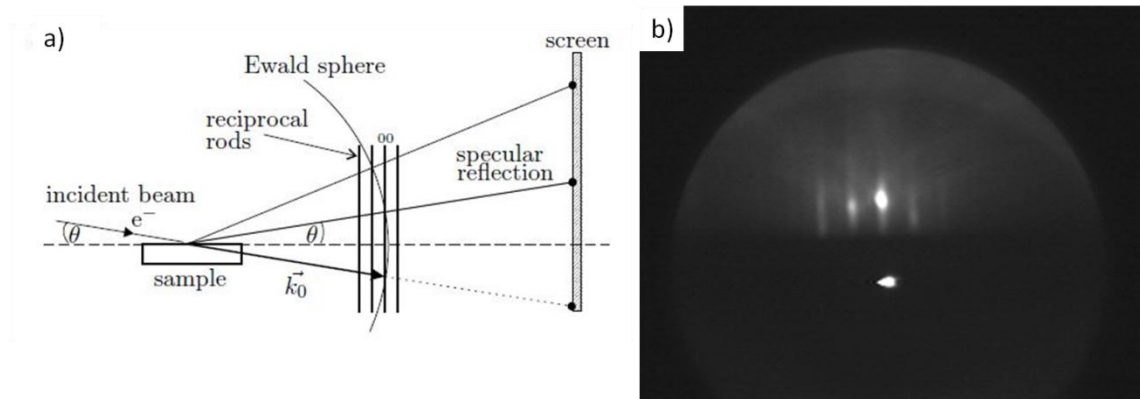


Figure 2-5 Schematic diagram of the study of film surfaces by RHEED. a) The sketch of the geometry of RHEED (Adopted from Ref.[57]), and b) RHEED pattern of SrTiO₃ substrate at ~720°C

In practice, the monitor of growing process is quite simple. One of the light spots of the RHEED pattern from reflected electron beam was first recognized, the intensity of it was then monitored. The intensity of recognized spot is proportional to the roughness of the detected surface. A higher intensity can be observed for a smoother surface. Figure 2-6 illustrates the above relation between roughness of the surface and the RHEED intensity of a period of homoepitaxial growth of a single unit layer of SrTiO₃.

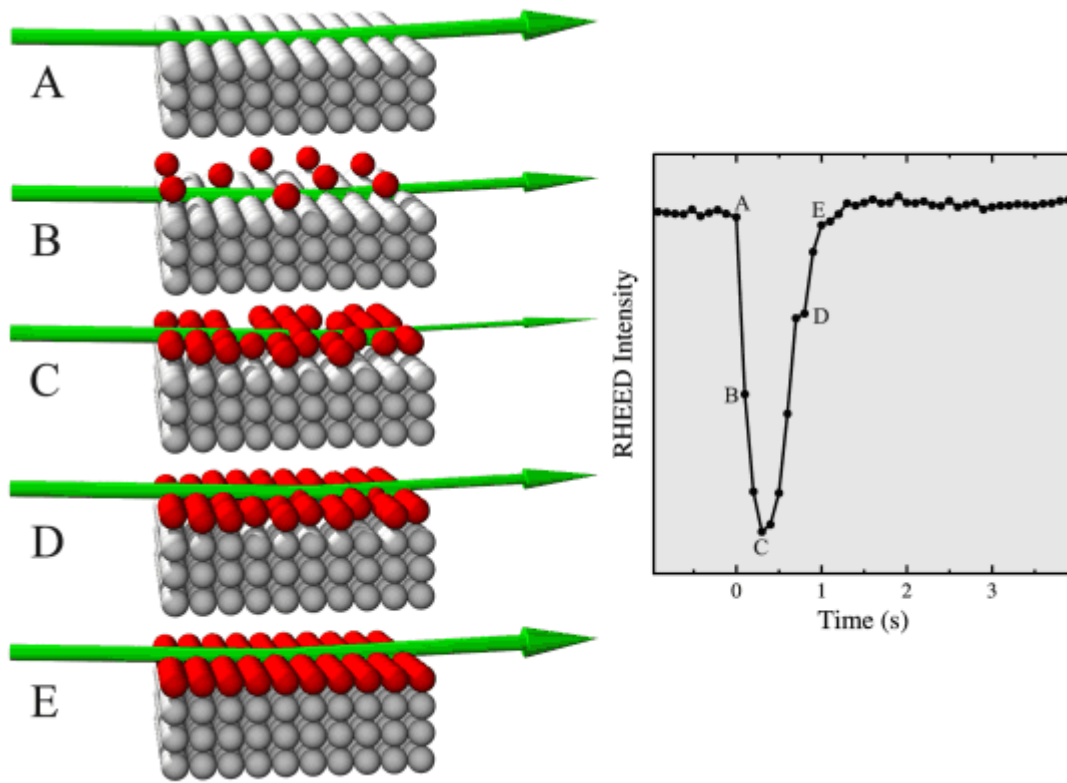


Figure 2-6 The surface models illustrating the growth of a single monolayer of film on a flat surface in layer by layer mode. The graph shows measured RHEED intensity during homoepitaxial growth of a single unit cell layer of SrTiO_3 (adopted from the website of RHEED company[65])

2.3.2 Surface Topography Examined by Atomic Force Microscopy

Atomic force microscopy (AFM), or scanning force microscopy (SFM), is a type of scanning probe microscopy with a very high resolution. The resolution of it can be demonstrated in the size of several nanometers or even in the order of angstrom, which is 1000 times better than the optical microscopy (optical diffraction limits the resolution of optical microscope). In addition, AFM is one of the foremost equipments achieving imaging, measuring, and manipulating matter at nanoscale. In AFM, the information is collected by a mechanical probe "touching" (utilize atomic force) onto sample surface,



THE HONG KONG POLYTECHNIC UNIVERSITY

and in order to provide the system with a tiny but accurate and precise movements allowing very precise scanning, piezoelectric scanners are used. In some variations, electric potentials can also be scanned using conducting cantilevers. In more advanced versions, currents can even be passed through the tip to probe the electrical conductivity or transport of the underlying surface.

The schematic diagram of AFM is shown in Figure 2.7 and the working principles of it are as following; the "soul" of it is a cantilever with a sharp tip at its end which is used to scan the sample surface. During the measurement, the sharp tip at the end of cantilever touches onto proximity of a sample surface. Then a deflection of the cantilever would be induced by forces between the tip and the sample. At the same time, the deflection would be measured using a laser spot reflected from the top surface of the cantilever into an array of photodiodes. Then, the information of photodiodes can be analyzed and the height of cantilever can be determined. Depending on the situation, by utilizing different types of tips, cantilever and the different additional equipment, many different types of forces and information could be measured in AFM including mechanical contact force, van der Waals forces, capillary forces, chemical bonding, electrostatic forces, magnetic forces, Casimir forces, solvation forces, etc.

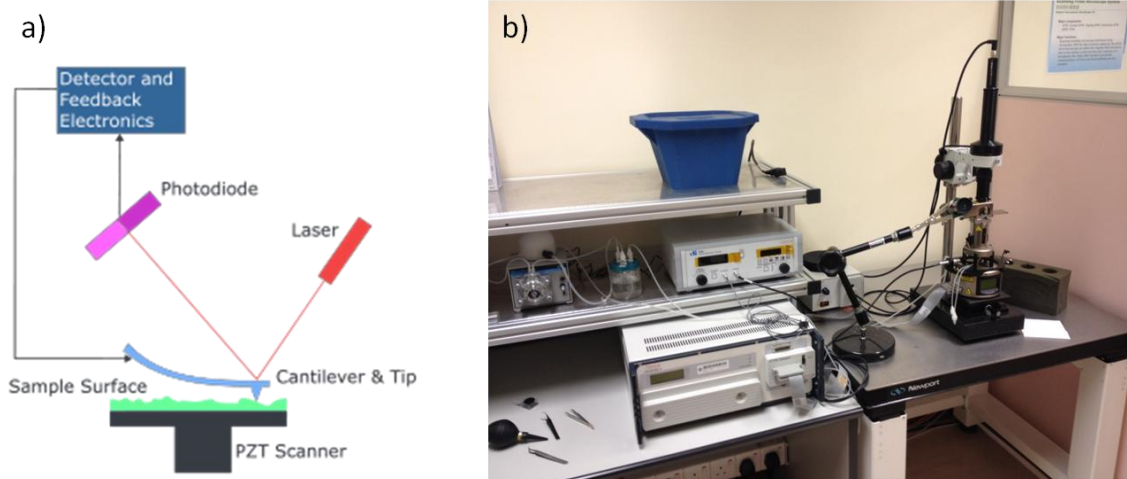


Figure 2-7 a) Schematic diagram of working principle of AFM (adopted from Ref.[66]), and b) The SPM system in our laboratory.

The AFM system can be operated in many different modes for different measurement. Each of them has its own advantages and disadvantages. In this thesis, AFM is mainly used to in basic contact mode and tapping mode in order to obtain the information of topography of samples.

2.3.3 Film Structural Characterization by TEM

Transmission Electron Microscopy (TEM) is a powerful microscopic tool for structural characterization even in an atomic scale. The examined material can be imaged by an electron beam transmitting through the sample or interacting with. As electrons need to transmit through the specimen, pre-treatment of the testing sample is needed. The sample has to be cut to a small piece and be grinded to ultra-thin. Many types of information such as mass, crystal structure, atomic number or defect of the sample can



THE HONG KONG POLYTECHNIC UNIVERSITY

be obtained. The Application of TEM imaging can be found in many different aspects like biological research, materials science and nanotechnology. In the thesis work, the high-resolution TEM (JEOL JEM-2010 TEM operated at 200kV) was use to confirm the structure and the number of layers of the samples.

2.4 Sensing Device Fabrication Techniques

2.4.1 Wire Bonding

After growing the epitaxial film and forming the heterointerfaces, the main problem is how to connect the conducting interface to measure its transport properties. There are a number of methods have been used. For example, in the first published work about the 2DEG in oxide heterointerfaces by Ohtomo *et al.*, laser-annealed ohmic contact through contact shadow mask to the interface was used [3]. Kalabukhov *et al.* made the connection by sputtering the gold pads on a Ti adhesion layer of the sample[67]. Thiel *et al.* used the Ar-ion etching and electrode patterning[57] technique for the connection. Huijben et al. used the wire bonder to connect the interface. In our work, the method of making the connection is same as Huijben by the wire bonding method. A piece of sample, mainly LAO/STO or other oxide further deposited on it, was first cut into the desired shape, and then the sample was mounted by the double-side tag onto the PCB. After that, bonding machine with aluminum wire (ASM AB510) was used to make the connection between the conducting interface and the copper on PCB (the LAO layer is only about 4 to 20 u.c. which is about 1.6 to 8 nm thick, therefore, the LAO layer will



THE HONG KONG POLYTECHNIC UNIVERSITY

be penetrated through by the aluminum wire and the conducting interface can be ohmic contacted to the aluminum wire). Finally, the transport properties of the heterointerface can be measured by contacting wires using silver paint or welding on the copper of PCB as shown in Figure 2-8.

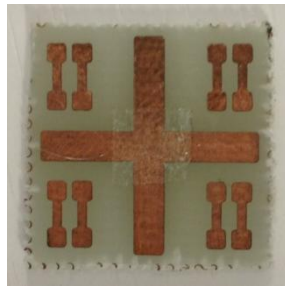


Figure 2-8 A photo of PCB. The double sided tag was placed at the centre and it is the position for the sample.

2.4.2 Parylene Coating

The name for parylene is for a variety of chemical vapor deposited poly (p-xylylene) polymers mainly used as moisture and dielectric barriers of different devices. Among the parylenes, Parylene C is the most popular one because of its combination of barrier properties, cost, bio-acceptable, and other processing advantages. [68]

In this work, during some of the measurements, samples need to be placed into water whereas short circuit will occur when metallic parts of the samples like aluminum wire and copper of PCB are in contact with the liquid. Therefore, Parylene coating is needed as an isolating layer. During the process, parylene was coated by the equipment called Parylene Deposition System 2010 as shown in Figure 2-9 (b).

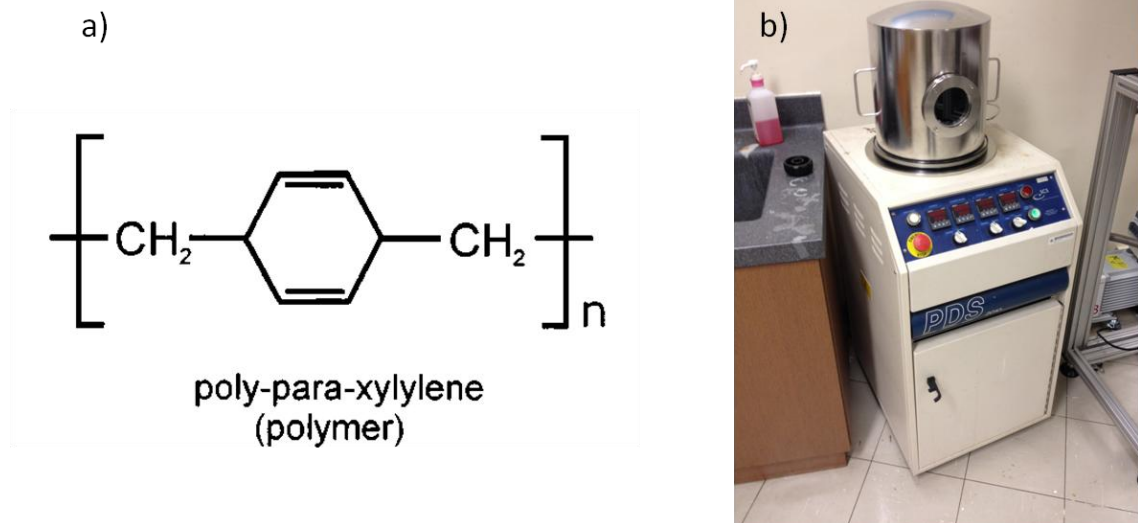


Figure 2-9 a) The chemical formula of parylene (Adopted from Ref.[69]), and b) is the equipment in our laboratory for parylene coating.

2.4.3 Patterning of the LAO/STO heterointerface

In this work, a long rod-shaped LAO/STO sample is needed for some kind of experiments. Photolithography is used for patterning as illustrated in Figure 2-10, and the pattern used was shown in Figure 2-11. The difficulty of the patterning is temperature limitation due to photoresist used, while the 2DEG is formed by epitaxial growth of LAO at about 750°C which is far beyond the temperature that photoresist can sustain.



THE HONG KONG POLYTECHNIC UNIVERSITY

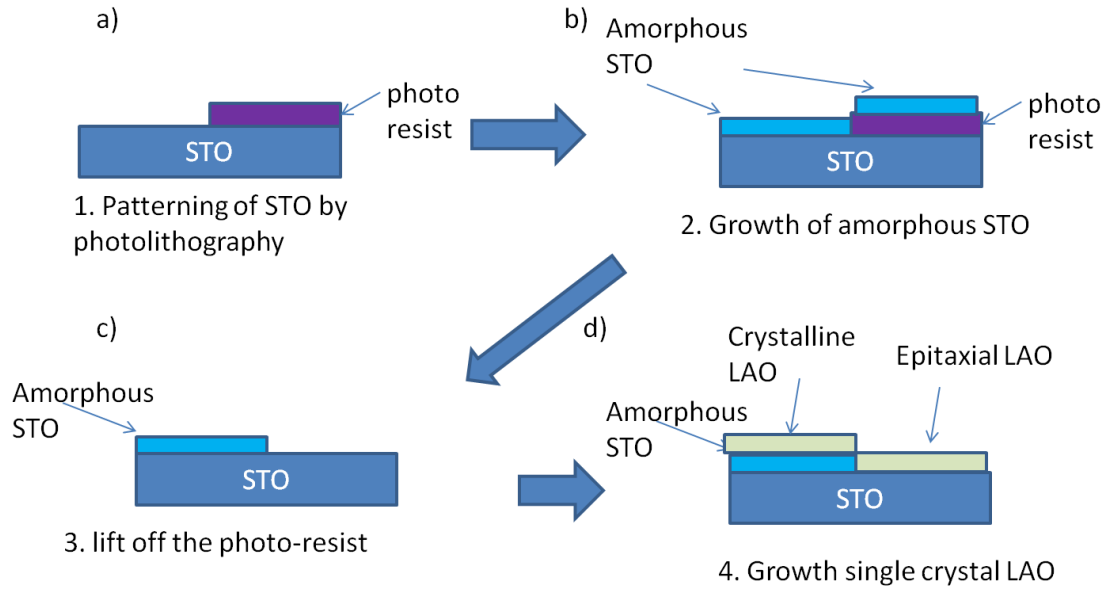


Figure 2-10 The basic representation of the patterning process: a) Patterning of STO by photolithography; b) Growth of amorphous STO; c) lift off the photo-resist; d) deposition of single crystal LAO at the designed temperature

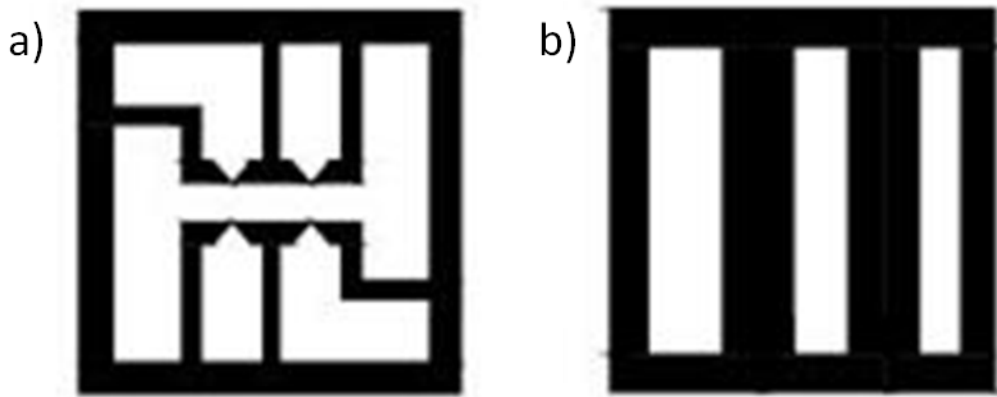


Figure 2-11 (a) and (b) Two main types of the patterns used in my work.



2.5 Measurement of Transport Properties

2.5.1 Sheet Resistance Measurement

In thin film electrical properties, a specific definition of resistance named as sheet resistance (R_s) is often used to probe the resistivity properties of the film. Instead of resistance R , sheet resistance R_s is widely used in thin film characterization because of its unique characteristics as a very thin layer which is close to a two-dimensional system. The resistance of a thin film is nominally uniform in thickness. By utilizing appropriate electrode geometries, sheet resistance, which is applicable to two-dimensional systems and analogous to resistivity used in three-dimensional systems, can be obtained from electric transport measurements. From fundamental electronics, we know that in a regular three-dimensional resistor, the resistance can be written as:

$$R = \rho \frac{L}{A} = \rho \frac{L}{Wt}$$

Where ρ is the resistivity, L is the length of resistor, and A is the cross-sectional area (of the resistor) which can be written as the production of the width W and the thickness t .

By combining the resistivity ρ with the thickness t , the resistance can be considered as:

$$R = \frac{\rho L}{t W} = R_s \frac{L}{W}$$

where R_s is the sheet resistance with the unit “ Ω/\square ” which means ohm per square.

From the above equation, R_s can be obtained by measuring the resistance of the materials using patterned sample with known ratio of L and W .



THE HONG KONG POLYTECHNIC UNIVERSITY

On the other hands, R_s can be obtained by another method which is Van Der Pauw (VDW)[70]. This method is commonly used to measure the sheet resistance of the material and Hall Effect. The method was firstly proposed by L. J. van der Pauw in 1958. Some of the shape and electrode configuration is shown in Figure 2-12. The sheet resistance R_s can be calculated by the following method. Firstly, the resistance

$R_{12,34} = \frac{V_{34}}{I_{12}}$ is calculated by the voltage between points 3 and 4 when the current source is applied to point 2 and point 3. The averaged resistance R is calculated

as $R = \frac{R_{12,34} + R_{34,12} + R_{21,43} + R_{43,21}}{4}$. Then, sheet resistance R_s is equal to $R_s = \frac{\pi R}{\ln 2}$.

Actually, Van Der Pauw method can also be used to calculate the sample with arbitrary sharp but it would not be mention in this thesis as samples used in my work are regular shape ($5 \times 5 \text{ mm}^2$).

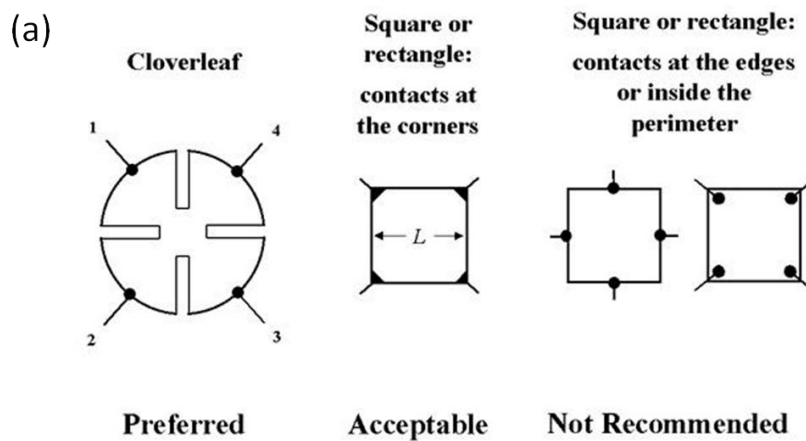


Figure 2-12 a) The electrode configuration of van der Pauw method(adopted from [71]).



2.5.2 Hall Measurement

Hall measurement is one of the methods to obtain the basic electric transport properties of the sample including: (1) sheet resistance R_s (with the help of van der Pauw method), charge carrier concentration n_s and Hall mobility μ . The principle of Hall Effect can be considered as following.

As shown in Figure 2-13, the current flows parallel to the applied electric field in a conventional conductor. However, if a magnetic field is applied perpendicular to the current, the current will experience a force called Lorentz force. The current flows to the side of the conductor and builds up a potential V_H . The calculations are as following: Hall voltage V_H is given by:

$$V_H = -\frac{IB}{ned}$$

where I is the current flows through the conductor, B the applied magnetic field, d the depth (thickness) of the plate, e the elementary charge, and n is the charge carrier density of the carrier electrons. The Hall coefficient is defined as:

$$R_H = \frac{E_y}{j_x B}$$

where j_x is the current density of the carrier electrons, and E_y is the induced electric field. So,



THE HONG KONG POLYTECHNIC UNIVERSITY

$$R_H = \frac{E_y}{j_x B} = \frac{E_y}{\frac{I}{dL} B} = \frac{dE_y L}{IB} = \frac{dV_H}{IB} = -\frac{1}{ne}$$

Therefore, carrier concentration n_s can be obtained. Since sheet resistance R_s has been calculated by Var Der Pauw method, the hall mobility μ can be calculated by:

$$R_s = -\frac{1}{n_s \mu e}$$

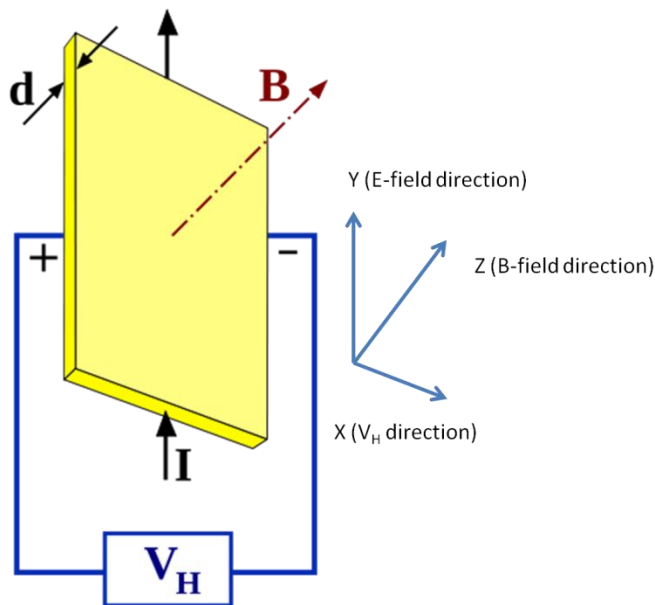


Figure 2-13 Schematic diagram of basic mechanism of Hall Effect (modified from [72])



Chapter 3 Characterization of LaAlO₃/SrTiO₃

Heterointerface

3.1 Introduction

The main task of this thesis work is to study the application of the LAO/STO 2DEG as a sensor, so it is essential to prove that the heterointerface grown has the 2DEG characteristics as reported in the literature. The characteristic property for the LAO/STO 2DEG is its metallic nature of conductivity at the interface and a reasonable value of carrier density and mobility. In this chapter the detailed processes of substrate treatment, thin film deposition, sample cutting and water-proof coating are introduced, and the transport properties of the heterostructure will be characterized.

3.2 Experimental Details

LaAlO₃ thin films were deposited by laser-molecular beam epitaxy (Laser-MBE) with a KrF excimer laser ($\lambda = 248$ nm) on TiO₂-terminated STO single crystal substrates [44, 46]. Prior to the deposition, the substrate was pre-cleaned by acetone and ethanol to remove any organic remnants on it. During the deposition, the substrate temperature was maintained at 750 °C and about 1×10^{-4} to 3 Pa O₂ pressure [73-75]. The growth was monitored by RHEED. The laser pulse repetition rate is 1 Hz. After deposition, the



THE HONG KONG POLYTECHNIC UNIVERSITY

samples were in-situ annealed under 10 mbar O₂ pressure for 1 hour at a reduced temperature of 550°C and then were cooled down to room temperature in the same ambient.

Atomic force microscopic topography confirmed that the step-terrace structure was maintained, indicating a good film quality. High-resolution TEM was employed to characterize the LAO/STO interface quality. The interfaces were contacted by aluminum wire using an ultrasonic wire-bonding machine for further transport properties measurements. Hall Effect was measured on samples with a Hall bar pattern. For rectangular samples, the central part was protected by a piece of tape (1 mm wide), and in order to isolate electrodes from liquids for sensor application, a parylene layer was subsequently deposited on top of the LAO film in a parylene deposition chamber. Current-voltage (I-V) characteristics were measured using Keithley 2400 source meter.



3.3 Surface Quality of Treated Substrates

3.3.1 Treatment Process

The method of surface treatment of STO substrate is introduced in Chapter 2, and the details are as following: (1) the commercial STO substrate was placed into a beaker filled with de-ionized (DI) water; (2) the beaker was placed into the ultrasonic bath for 20 min; (3) the substrate was dried by compressed air steam (CAS); (4) the dried substrate was immersed into buffered-HF solution (NH_4F : HF=7:1) for a certain time of period; (5) the substrate was ultrasonically cleaned by DI water and ethanol for 10 min, respectively; (6) the substrate was dried by CAS; (7) the substrate was annealed in pure oxygen ambient at 1000°C for 1 or 2 hours.

3.3.2 Topography of Substrate Surface

After the surface treatment process previously mentioned, the sample was measured by AFM. The sample topographies for different etching conditions are shown in Figure 3-1. From these images, we can find that the exposed time to BHF should be about 60s to 90s, and the height of the terrace is about 0.4 nm, demonstrating that the steps are one unite cell high, i.e., the surface layer is either Ti-terminated or Sr- terminated. It is also apparent that there are some bright spots at the edge of the steps. These spot defects are



THE HONG KONG POLYTECHNIC UNIVERSITY

believed to be due to the crystal defect pinning to the etching process. Details of the formation mechanism needs further study.

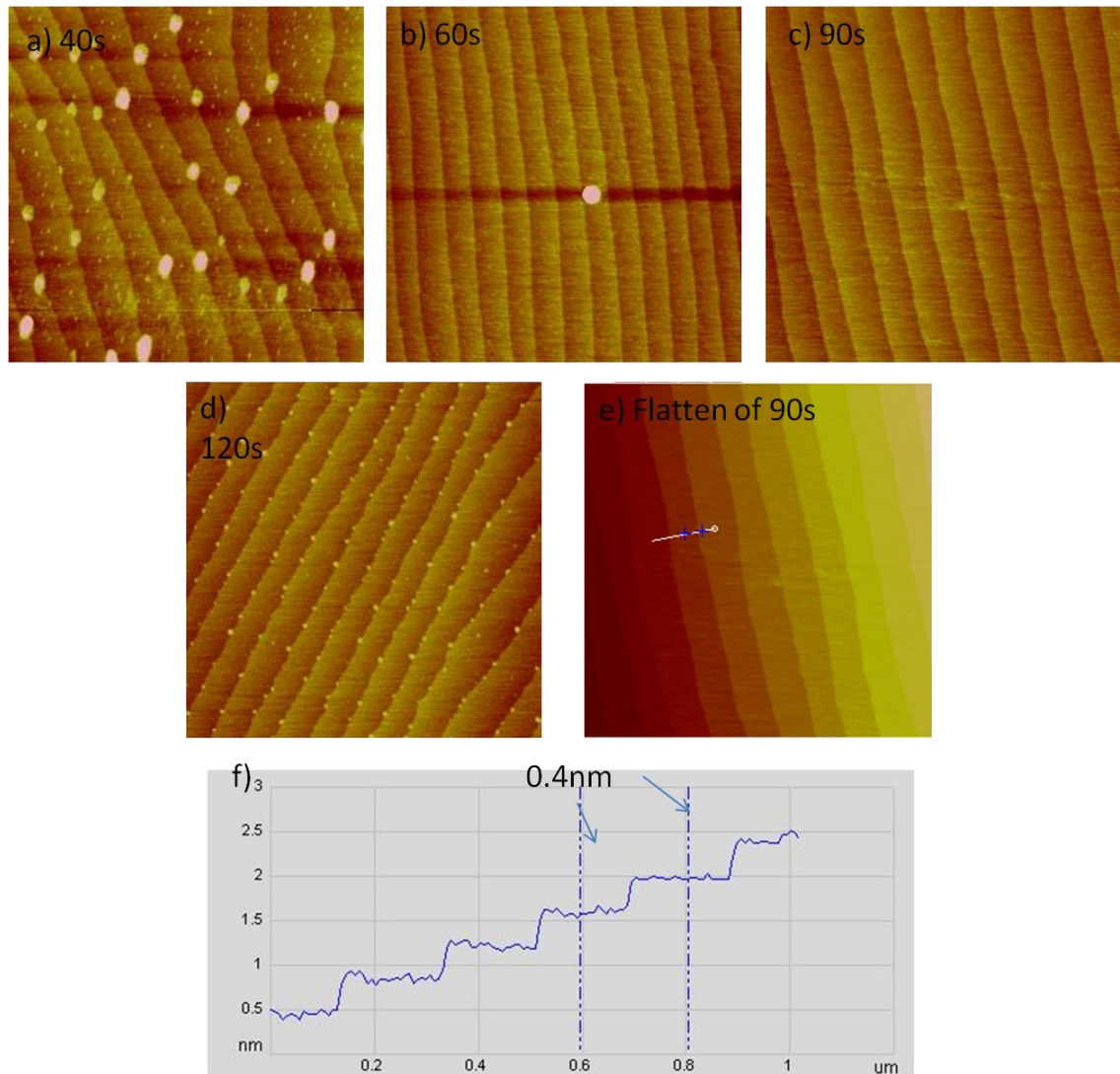


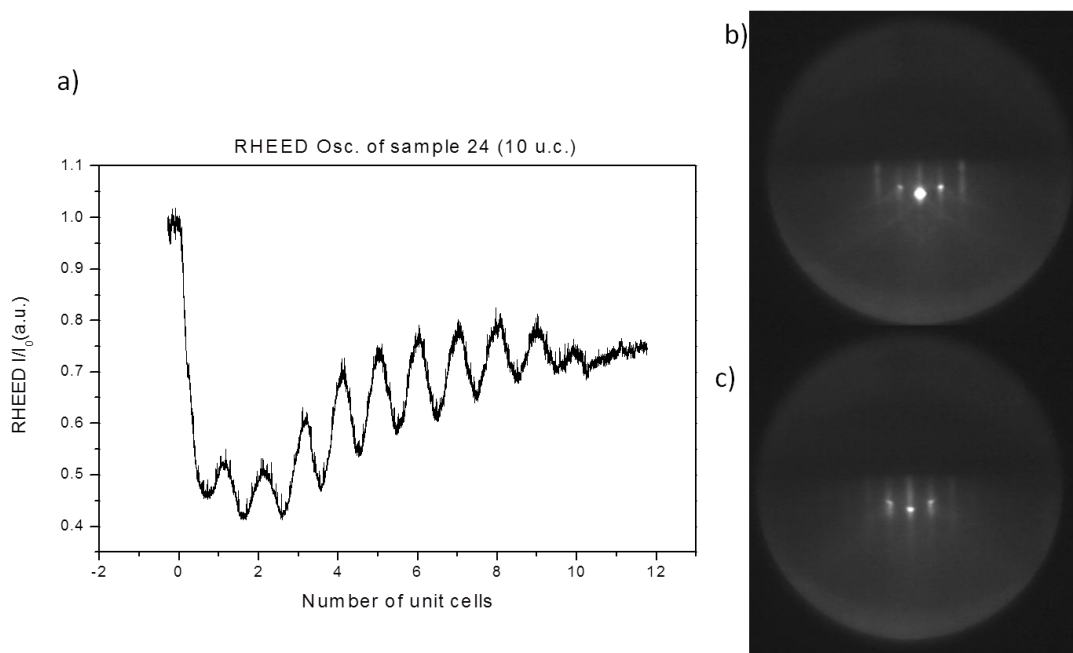
Figure 3-1 AFM image of the treated STO substrate. The size of AFM images are $2 \times 2 \text{ um}^2$: a) 40s etching by BHF; b) 60s etching by BHF; c) 90s etching by BHF; d) 120s etching by BHF; e) the flatten AFM image of (c); f) the surface profile of (e) showing vertical distance of the terrace of about 0.4 nm.



3.4 Structural Properties of LAO/STO Heterostructures

3.4.1 Growth Process Monitored by RHEED

The deposition was in-situ monitored by RHEED system. The RHEED pattern of treated STO substrate prior to deposition at 750°C was shown in Figure 3-2(b), where the spot of the pattern presents a perfect substrate surface. Figure 3-2(c) is the RHEED pattern after 660s deposition of LAO which is the end of the deposition. The RHEED oscillation of spectrum reflection during the deposition of LAO is shown in Figure 3-2(a). The periodic signal demonstrates the number of unit-cell layers formed on the substrate.





THE HONG KONG POLYTECHNIC UNIVERSITY

Figure 3-2 RHEED pattern and the oscillation of the intensity: a) the oscillation of intensity of the RHEED pattern during the deposition of LAO on STO substrate; b) RHEED pattern of treated STO substrate prior to deposition at 750°C; c) RHEED pattern after 660s deposition of LAO which is the end of the deposition.

3.4.2 Structure of thin films and interfaces

In order to confirm the LAO film thickness and exam the quality of the film and interface, cross-sectional high-resolution TEM imaging was carried out. Fig. 3-3 (a) shows the HRTEM image of the LAO film on STO and Fig 3-3 (b) is a magnified image where the atomic resolution structure can be clearly seen. From the image, it can be found that the LAO film is epitaxially grown on SrTiO₃ substrate, and interface is sharp and smooth; while the thickness of the LAO film is about 9-10 u.c. which is very close to the nominal thickness of 10 u.c. determined from the RHEED intensity oscillation result.

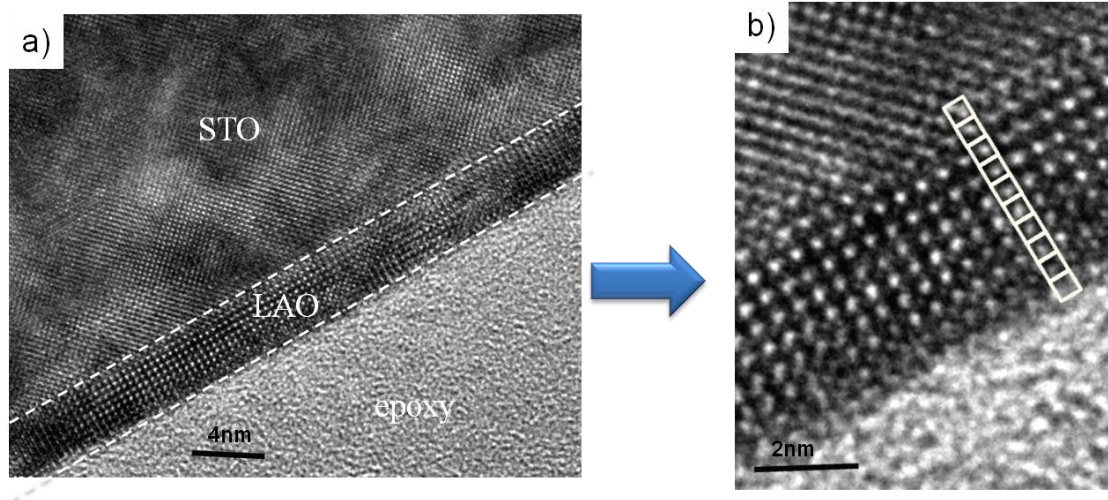


Figure 3-3 (a) High-resolution TEM image of the LAO/STO interface, and (b) an enlarged image of (a). The number of unit-cell (9-10 u.c.) can be counted just as expected from RHEED intensity oscillation result.



3.5 Electrical Transport Properties

In order to measure the electric transport properties of the LAO/STO heterointerface, wire bonding technique was used to make the contact in a Var Der Pauw pattern. The optimized bonding parameters are shown in Table 3-1. It is worth noting that it is easier to bond the sample by choosing the copper pad on PCB as the first point and oxide surface the second one.

Table 3-1 the parameters used for wire bonding of standard sample

First bond reference (copper of PCB)	
First bond Power	130
First bond Time(ms)	90
First bond Force(g)	35
Second bond reference (oxide surface)	
Second bond Power	140
Second bond Time(ms)	50
Second bond Force(s)	50

After connecting the interface and the copper pad on PCB, the interfacial electric transport properties were measured using Lakeshore Hall measurement system and a cryogenic stage combined with Keithley source meters, HMS-5000 Hall effect measurement system with variable temperature from 80 to 350 K (ECOPIA) and physical property measurement system (PPMS).



THE HONG KONG POLYTECHNIC UNIVERSITY

All chosen samples shared similar electric transport properties with slight variation. The temperature-dependent sheet resistance and mobility of the measured LAO/STO sample are shown in Figure 3-4, from which the magnitude of sheet carrier density can be determined as n-type with $n_s = 10^{13} / \text{cm}^{-2}$ and the highest mobility reaches $2 \times 10^3 \text{ cm}^2 \text{V}^{-1} \text{s}^{-1}$ at 2.5K.

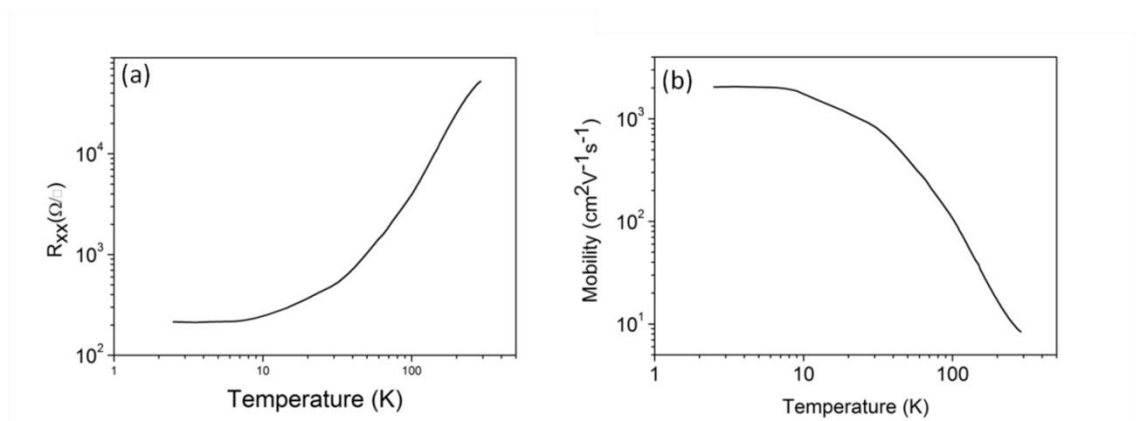


Figure 3-4 Temperature-dependent sheet resistance (a), and mobility (b), of the LAO/STO interface.

By comparing growth condition and the basic transport properties to the literature [301], we can conclude that our samples have very similar 2DEG characteristics and are ready for further study in sensing device application.



Table3-2 Values of electric transport properties reported in different studies, where the data in this table are all taken at low temperature about 5 K (adopted from Ref.[76]).

Growth p_{O_2} (mbar)	annealing conditions	R_s (Ω/\square)	n_s (cm^{-2})	μ_H ($cm^2 V^{-1} s^{-1}$)
10^{-6}	not annealed	10^{-2}	10^{17}	10^4
10^{-6}	annealed in 1 atm of O_2 at 400°C for 2 hours	10^{-2}	2×10^{16}	10^4
10^{-6}	not annealed	10^{-2}	5×10^{16}	10^4
10^{-6}	annealed at 500 mbar during cooling	10^2	10^{13}	10^3
10^{-6}	annealed at 300 mbar during cooling	10^2	3×10^{13}	7×10^2
10^{-6}	not annealed	3×10^{-3}	—	10^4
10^{-6}	not annealed	—	2×10^{16}	10^4
10^{-5}	not annealed	10^2	10^{16}	10^0
10^{-5}	not annealed	10^{-3}	5×10^{17}	2×10^3
2×10^{-5}	cooled at high oxidation	—	2×10^{13}	3×10^2
10^{-4}	not annealed	10^4	10^{14}	10^1
10^{-4}	not annealed	10^2	10^{13}	10^3
10^{-4}	annealed at 500 mbar during cooling	10^2	10^{13}	10^3
10^{-4}	not annealed	3×10^{-3}	—	10^1
5×10^{-2}	not annealed	insulating	insulating	insulating
$10^{-6} - 10^{-3}$	annealed at 300 mbar during cooling	insulating	insulating	insulating

3.6 Water-Proof Sample Preparation

During the measurement, the samples need to be put into different liquids or in contact with liquid. Since the conductivities of many polar liquids (such as water, acetone or ethanol) are comparable to the 2DEG, when polar liquid is in contact with the aluminum wires on both sides of the sample, a significant proportion of the current may pass



THE HONG KONG POLYTECHNIC UNIVERSITY

through the polar liquid and induces the short circuit which should affect the results of the experiment. Therefore, to make water-proofed sample is important for those experiments. In Chapter 2, parylene coating was introduced to achieve the goal of water-proofing. Parylene is a type of polymer that has little effect to the transport properties of the sample and can also provide a high resistance protection layer to the LAO surface, copper on PCB and aluminum wire of connection. In order to show that parylene is suitable for this purpose, I-V curves of a standard sample at room temperature before and after parylene coating were recorded as shown in Figure 3-5. It is apparent that the I-V curve has very little change when the parylene coated sample is put inside water.

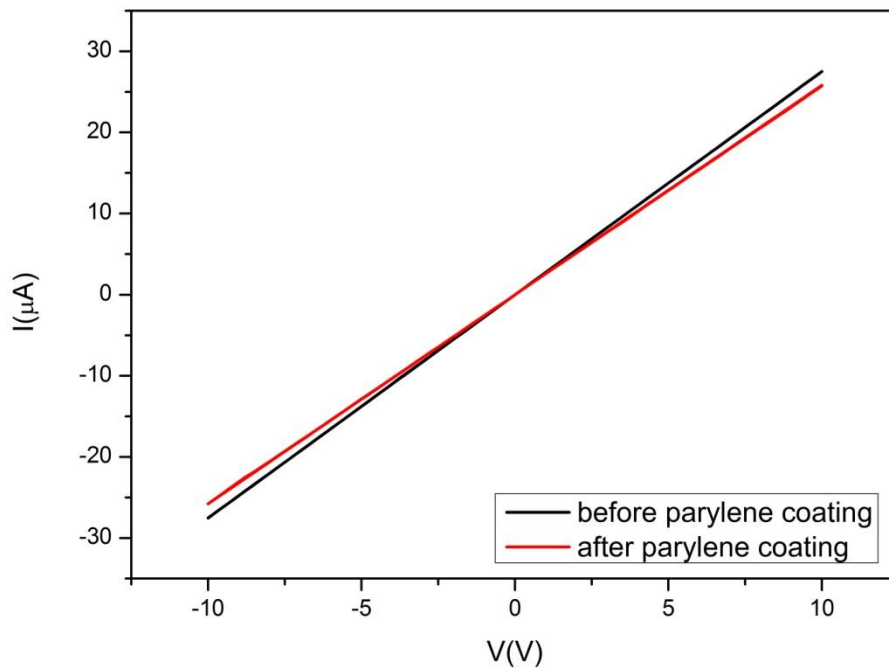


Figure 3-5 I-V characteristic of the standard sample before and after parylene coating (total surface coated)



The procedure of preparing water-proofed samples and the photo of prepared sample are shown in Figure 3-6 and 3-7, respectively. Basically, a piece of desired shape of sample was mounted onto a PCB board and the connections between the LAO/STO interface and copper pad on PCB were made by wire bonding (shown in Figure 3-6(a) to (c)). After that, a piece of blue tape with 1mm wide was placed onto the centre of the sample, and finally, the sample was put into the parylene coating system, and the blue tape was peeled off after parylene coating to obtain the water-proofed sample with an opened window for the LAO thin film that can be used to sense polar liquids etc.

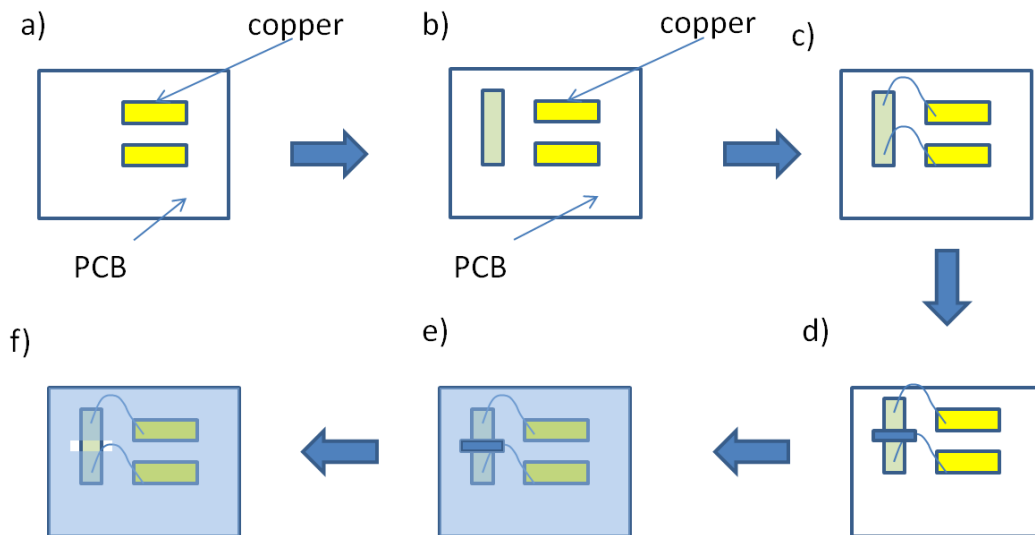


Figure 3-6 Schematics diagram of the process of the water-proof sample: a) a piece of bare PCB; b) a piece of sample with the shape of long rod pasted onto the PCB; c) the connection between the copper on PCB and the conducting interface by bonding machine (ASM AB510); d) a blue tape was placed at the centre of the sample; e) the sample coated by the parylene; f) peel off the blue tape to obtain the open window for testing.

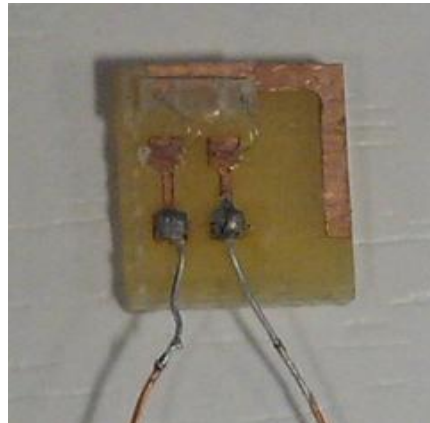


Figure 3-7 Photo of the standard water-proof sample

3.7 Summary

In this chapter, the process of fabricating LAO/STO (with substrate treatment) thin film has been shown. RHEED, TEM and AFM have been used for the characterizations of the LAO thin film. Electric transport properties of the LAO/STO heterointerface were measured and the results show that 2DEG has been successfully formed at the LAO/STO heterointerface. The water-proofed sample has also been synthesized and the results show that it is ready for sensor device application.



Chapter 4 Polar Liquid Molecule Induced Transport Property Modulation at $\text{LaAlO}_3/\text{SrTiO}_3$ Heterointerface

4.1 Introduction

In the polar-catastrophe model [3, 7], a proposed charge transfer from LAO layer (including surface) to the interface is associated with a built-up of the internal electric field in the LAO layer originating from the polar discontinuity between LAO (alternating charged layers) and STO (charge-neutral layers). Such an internal electric field was also predicted from first-principle calculations for STO/LAO/vacuum stacks,[28, 30, 77-79] and illustrated by various experimental evidence[39, 80, 81]. For example, a latest experimental observation of an lattice expansion along the LAO c-axis in ultra-thin layers indicated a strong electrostrictive effect produced by dielectric LAO[82]. Recent experimental reports also clearly revealed the importance of the correlation between the interface and the surface charge states. Therefore, the interfacial conduction was able to be manipulated using a conducting atomic force microscopy technique [11, 12] through playing with the surface charges and adsorbates [83-85], or a capping layer of STO [86]. The fact that the interface conducting states can be dramatically sensitive to the surface adsorbates leads to a strong potential of LAO/STO interfaces functioning as polar molecule sensors.



Most recently, Xie et al. [16] reported the surface adsorption of polar liquids, such as water, induced large change (by a factor of three) in the conductivity at the LAO/STO interfaces. This conductivity change has been attributed to an increase of sheet carrier density of the 2DEG by more than $2 \times 10^{13} \text{cm}^{-2}$, suggesting that the adsorbates have a great influence on the charge transfer from the film surface to the interface. These results also suggest that sensor application is possible by utilizing the surface-interface coupling induced conductivity modulation. In this chapter, room-temperature current-voltage (I-V) characteristics of the LAO/STO interface are studied using an in-plane field effect transistor (FET) device structure, whereas the polar molecules act as a gate voltage to affect the source/drain current across the interface channel. The local conductivity of the buried interface dramatically changes from metallic to semiconducting when a droplet of the polar liquid such as water is put onto the film surface. These observations provide a direct evidence of the build-in electric field in LAO layer and demonstrate that such a fascinating interface system can be used for high-performance polar molecule sensors.

4.2 Polar Sensing

I-V characteristics of the LAO/STO interface were measured before and after placing a droplet of liquid at the center of the sensor. A variety of liquids, including water, acetone, gasoline, hexane etc., have been tested. Figure 4-1(a) shows the I-V curves with and



THE HONG KONG POLYTECHNIC UNIVERSITY

without a water droplet on top of the LAO surface. It can be seen that for the sample tested in air, the I-V characteristic is typically linear with perfect ohmic behavior, illustrating a metallic conduction at the LAO/STO interface. However, when a drop of water is added to the exposed LAO surface, the I-V curves change to a typical FET source-drain type current with a strong saturation at high voltages. This metal/semiconductor/metal junction-like behavior indicates that, there is a strong field effect induced by water molecules that changes the local interfacial conduction from metallic to semiconducting. Such similar junction characteristic has been observed in the LAO/STO 2DEG in contact with semiconductors or insulators. [40, 87, 88] Since LAO is a polarized ionic oxide with the polarization pointing from the substrate to the surface[16], water molecules which are polar, have a tendency to align their dipole moments with the electrostatic field to reach the most stable state (Fig. 3-8 (b)). As also illustrated in Ref. [16], the water molecules' alignment weakens the local electric potential in LAO and thus modifies the band structure of LAO. We believe that for our sample with water droplet on top of LAO surface, the weakening of the local electric field in the LAO layer underlying the water droplet results in a transition of the interfacial transport property from metallic 2DEG to n-type semiconducting dominated, as shown in Fig.4-1(b). Therefore, a metal/n-type semiconductor/metal junction, analogous to a narrow channel field-effect transistor, can be formed, whose I-V characteristic far deviates from linear relation. The liquid was kept present on top of the sample surface while the measurements were performed. It is noticed that by blowing off all visible liquid immediately after placing the droplet, the I-V curve recovers to perfect ohmic behavior with a smaller resistance. After the sample was heated to above



THE HONG KONG POLYTECHNIC UNIVERSITY

373 K, the linear I-V characteristics can be resumed. We also note that non-polar liquids such as gasoline and hexane have no obvious influence on the I-V curve (not shown since they are exactly the same as that without water droplet).

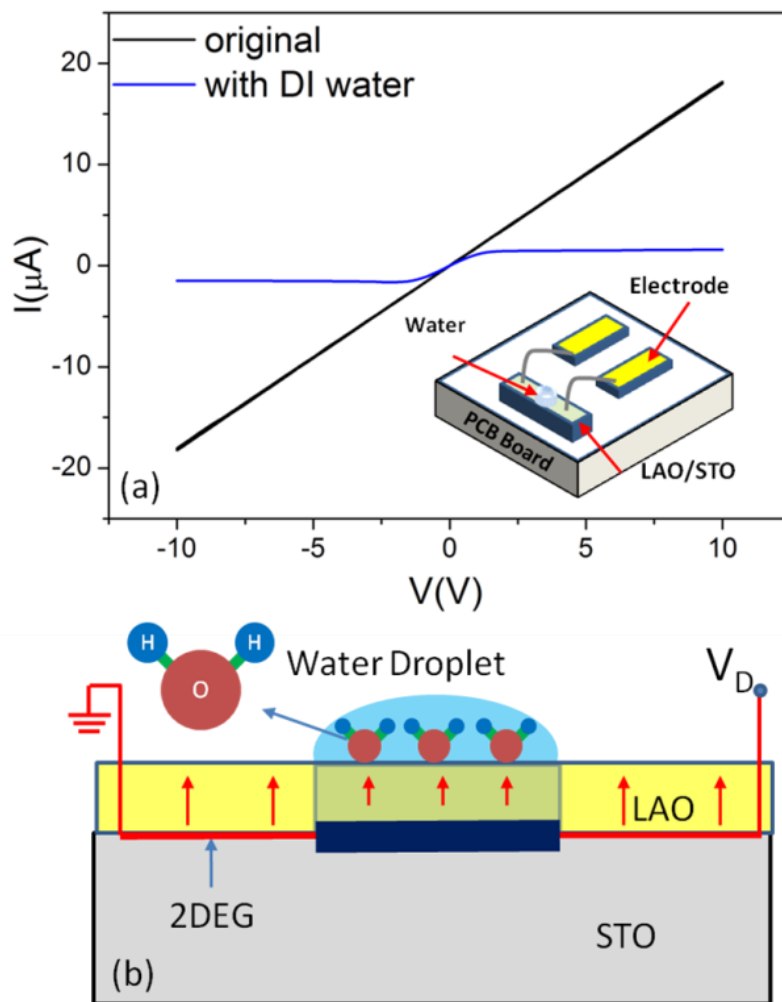


Figure 4-1 (a) I -V curves of the LAO/STO interface with/without water droplet on top of LAO surface. The inset is a schematic diagram showing the sensor structure. (b) Schematic diagram illustrating water molecule alignment along the electrostatic field direction on the sample surface. The larger arrow indicates relatively larger polarization field, and the smaller arrow represents smaller polarization field in the LAO layer.

4.3 Schottky Diode-Like Junction

It is interesting to see that the 2DEG is sensitive to the position of water droplet on the LAO surface. When the water droplet is placed off from the device center (for this experiment, there is no insulating parylene coating), the I-V curve becomes asymmetric. Figure 4-2(a) shows a rectified I-V curve when the water droplet is close to one side of the electrodes. It is believed that a Schottky diode-like junction is formed in this polar molecule modulated oxide interface, and a schematic diagram is shown in Fig.4-2(b) to illustrate the mechanism of forming the Schottky junction.

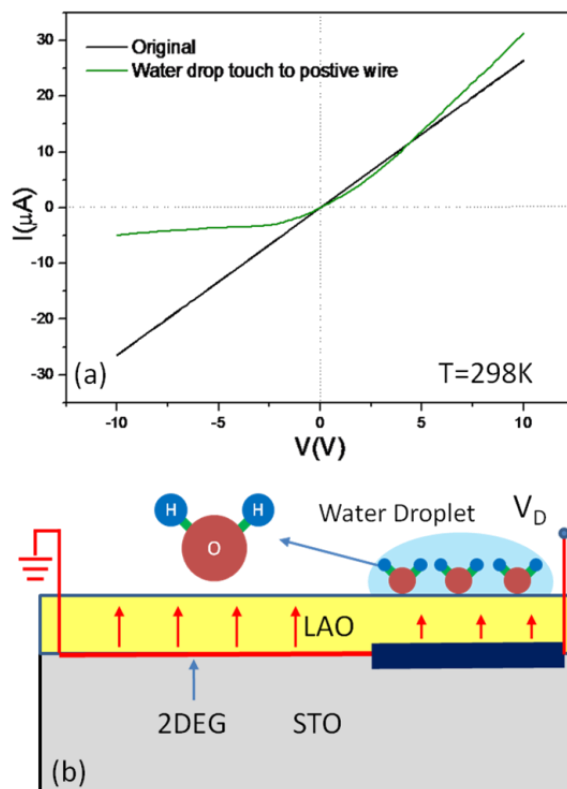


Figure 4-2 (a) I -V curves of the LAO/STO interface with water on top of LAO surface but close to one end of electrode, and (b) schematic diagram illustrating water molecule alignment along the electrostatic field direction on the sample surface.



4.4 Schottky Junction Composed of Metal and n-Type Semi-Conductor

To explain the mechanism of the formed junction, the basic properties of Schottky junction are introduced. Different junctions will be formed due to different properties of those materials, when a type of semi-conductor contacts to another type of semiconductor or contacts to a metal. A Schottky junction is a type of junction formed by a metal contacting with a semiconductor material. The key to understand the behavior of the Schottky junction is to consider the work function of the semiconductor Φ_s and the work function of the metal Φ_m in terms of the following two cases:

Case 1:

If the work function of the metal Φ_m is larger than the work function of the n-type semiconductor Φ_s , considering $\Phi_m > \Phi_s$ shown in Figure 4-3, Schottky barrier would be formed. Since in thermal equilibrium, the Fermi level of the whole system has to be the same, electrons should flow from the semiconductor into the metal due to the lower energy states in metal. Then remaining positively charged donor atoms in the semiconductor create a space charge region. The potential barrier seen by electrons in the metal side trying to move into the semiconductor is known as "Schottky barrier".[89]

If a positive bias is added onto the semi-conductor side (shown in Figure 4.3 c),



THE HONG KONG POLYTECHNIC UNIVERSITY

the electrons will try to flow from the metal side to semiconductor side. However, most of the injecting electron included by the bias would be blocked by the Schottky barrier. Therefore, the rectifying behavior occurs. On the contrary, if a positive bias is added onto the metal side (shown in Figure 4.3 d), the electrons will try to flow from the semiconductor side to the metal side. In this situation, a part of bias potential is used to compensate the barrier voltage Φ_{bi} , which is equal to the difference of Φ_m and Φ_s , and the rest bias induces the electrons crossing the junction like an ohmic contact. The I-V characteristic of such contact is shown in Figure 4-4.

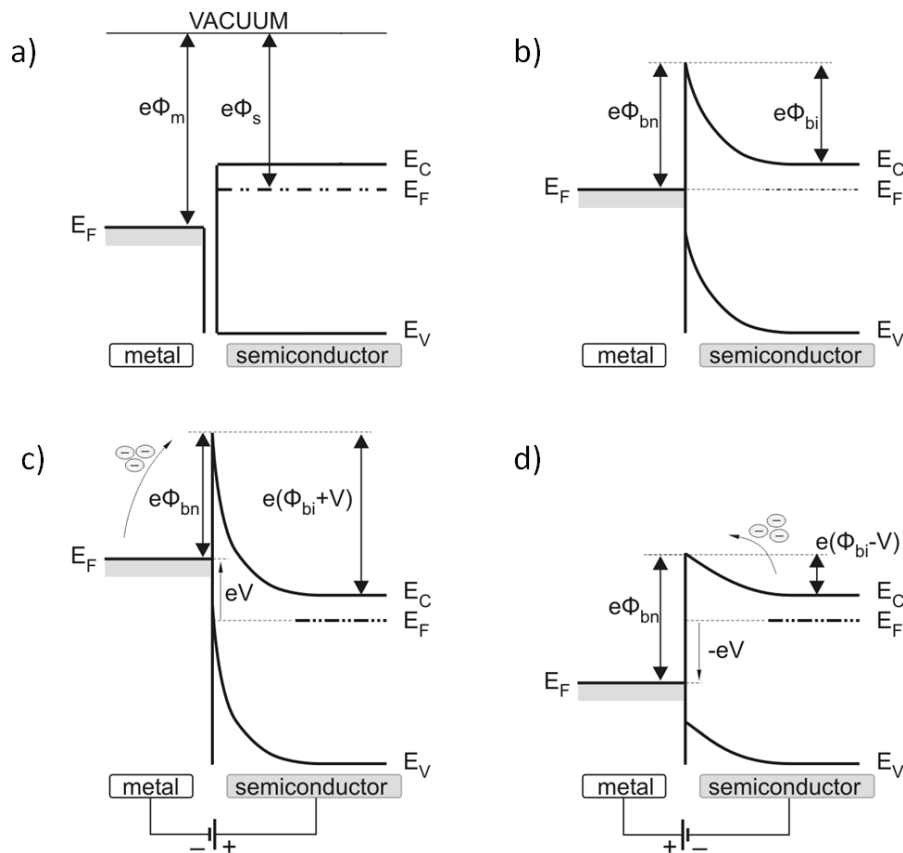


Figure 4-3 Energy-band diagrams of a metal with a higher work function in contact with a n-semiconductor: (a) before contacting, (b) after contacting in equilibrium, (c) under reverse bias and (d) under forward bias. (Modified from Ref. [89])

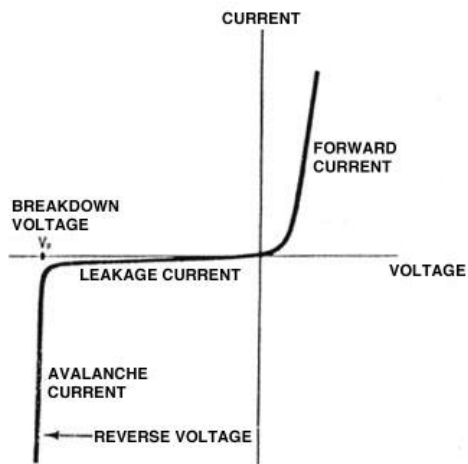


Figure 4-4 I-V characteristic of the Schottky junction forming by the contact of metal and n-type semiconductor. The work function of metal is relatively larger. (Adopted from Ref. [90])

Case 2:

If the work function of the metal Φ_m is lower than that of n-type semiconductor Φ_s , i.e., $\Phi_m < \Phi_s$ as shown in Figure 4.5, an ohmic contact will be formed. In the thermal equilibrium, the Fermi level of the whole system has to be the same, so electrons should flow from the metal into the semiconductor due to the lower energy states in semiconductor. Although, losing some electrons, the number of electrons in the metal side is still much more than electrons in the semiconductor side. The band of metal remains unchanged. In this case, when a bias is added on to the system, whatever the direction of the bias, electron can flow freely passing through the junction. Therefore, it is regarded as the ohmic contact.

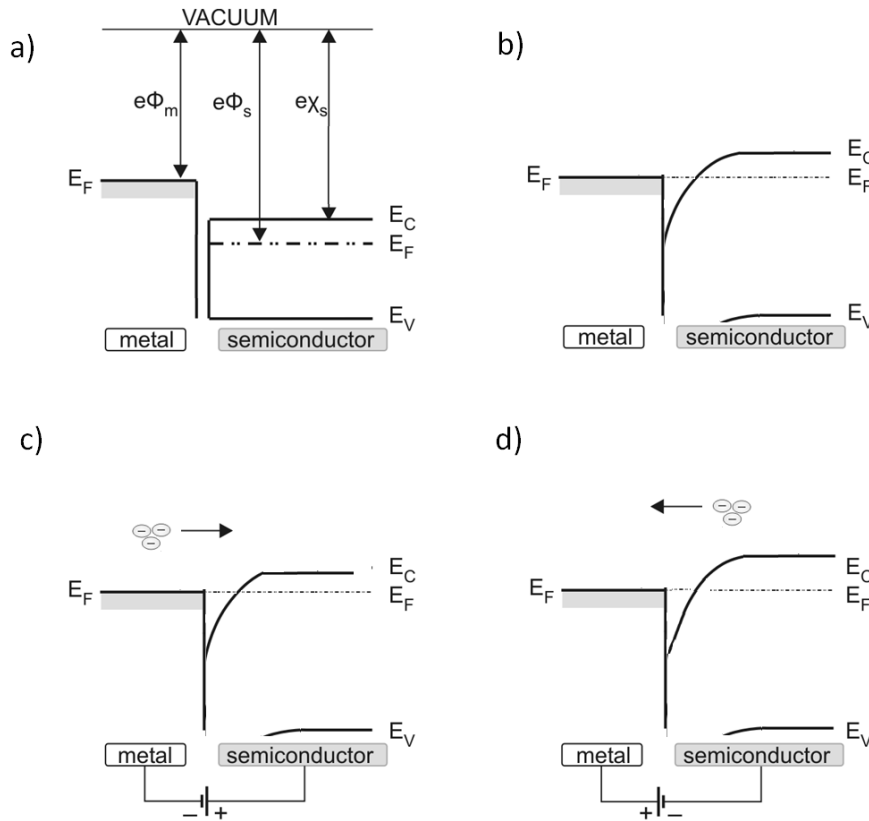


Figure 4-5 Energy-band diagrams of a metal with a lower work function contact to n-semiconductor: (a) before contacting, (b) after contacting in equilibrium, (c) and (d) are different direction of the bias.

4.5 Proposed Explanation of the Behavior

Figure 4-6 illustrates the band diagram qualitatively demonstrating the proposed conducting mechanism across the junction of the 2DEG and n-type semiconducting LAO/STO interface under the water droplet. Figure 4-6 (a) shows the state when water droplet is placed at center of the sensor without adding V_D , where two Schottky junctions are formed; while under V_D , the band structure changes, and the current is



THE HONG KONG POLYTECHNIC UNIVERSITY

restricted by the thickness of the depletion layer through a tunneling mechanism (Fig. 4-6 (b)). For the case when water droplet is placed at one side closing to the electrode, where one Schottky junction is formed between the metallic and n-type semiconducting LAO/STO interface, the current is rectified. Figures 4-6(c) and (d) demonstrate the band structure of this junction. One can see that there is no saturation observed when the positive V_D is applied. This indicates that, for the 2DEG, the Fermi level of the metallic region is higher than that of the n-type semiconducting region, which is different from a typical Schottky diode [91]. The typical charge carrier density of 2DEG at the LAO/STO interface, usually with a value of $\sim 10^{13} \text{ cm}^{-2}$, is much lower than normal metals, as a result, a non-negligible local depletion layer in metallic 2DEG region can be formed near to the junction. In this scenario, when $V_D > 0$, as shown in Fig. 4-6 (c) (2DEG is negatively biased), the depletion layer in the metallic region is suppressed. Therefore, a quasi-ohmic behavior can be observed. While for $V_D < 0$, as shown in Fig. 4-6 (d) (2DEG is positively biased), the current is likely to be limited due to the locally-formed barrier in metallic region. As a consequence, a “rectifier” is realized.

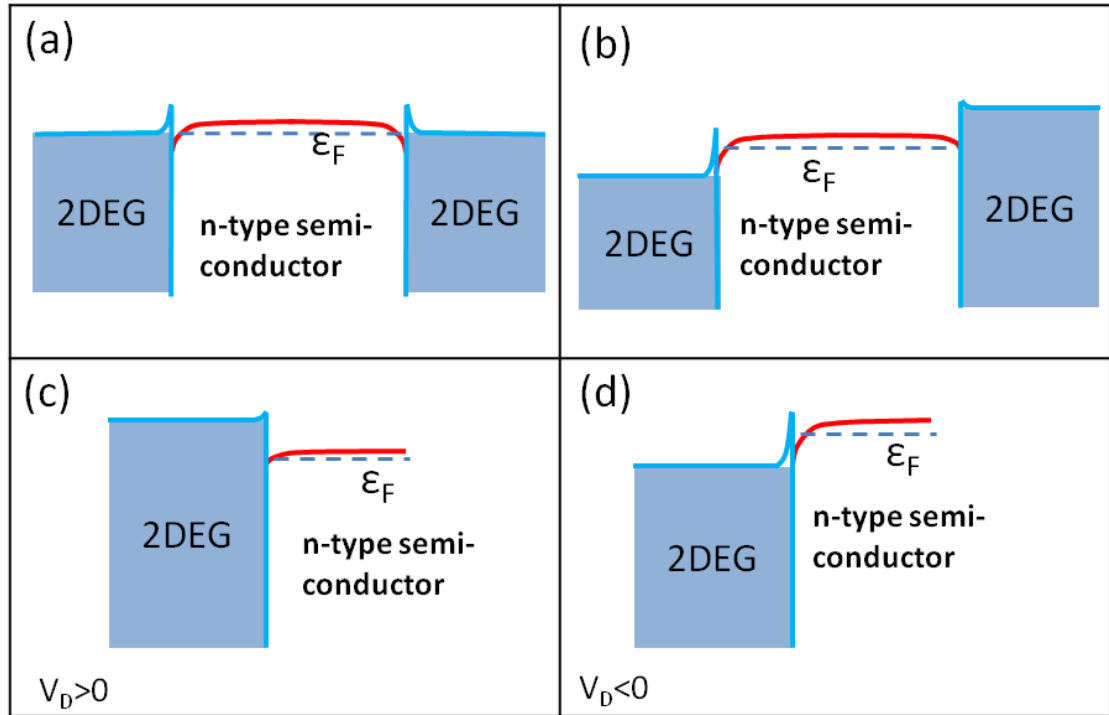


Figure 4-6 Schematic band diagrams for the Schottky junctions formed along the LAO/STO interface of the sample with water droplet in the center of the sample for, (a) zero bias voltage, and (b) non-zero bias voltage. (c-d) Schematic band diagrams when water droplet is close to one side electrode: (c) when $V_D > 0$, and (d) when $V_D < 0$.

It is worthy to compare our work to Ref [16], where it was demonstrated that water absorption at the LAO surface increases the sheet carrier density at the interface after the water droplet was blown off. Our results are different to Ref.[16] in terms of the following aspects. The work in Ref. [16] addressed a common problem existed in the 2DEG characterizations where the samples usually are not virgin, i.e. has been “contaminated” by water, and therefore, the charge carrier density has been increased but still metallic. While in our work, the sample has been contaminated by water during sample cutting, mounting with wax and acetone cleaning process etc. But our result is a



THE HONG KONG POLYTECHNIC UNIVERSITY

real approach toward sensors applications when the surface is presented with liquids, such as water or DNA solution etc. Our experiments reveal that the 2DEG changes to n-type semiconductor when polar water molecule present at the LAO surface, i.e. a phase change of transport; while in Ref[16]'s work, the transport is still metallic in nature, but with an increase of sheet carrier density. We attribute this significant difference to the very different experimental methods we used. In our case, the modification to the 2DEG transport property is by a large number of layers of water molecules; while in Ref [16] work, water was blown off before the measurement, so the surface is only covered by very limited layers of water molecules. In addition, our results reveal transport properties across a Schottky junction between the 2DEG and n-type semiconductor; while there is no junction involved in Ref. [16] since the whole area is "covered" by water molecules. The existence of a junction not only reveals the nature of the 2DEG transport tuned by water, but also other characteristics such as their work function relative to the n-type semiconductor.



4.6 Other Work

Polar liquid molecule induced transport property modulation at $\text{LaAlO}_3/\text{SrTiO}_3$ heterointerface has been demonstrated and a model has been proposed to explain the observed phenomena. In this session, some preliminary results of extended work based on the same idea of modulating the transport property of the 2DEG through field effect for sensing application are introduced.

4.6.1 Polar Liquid Molecule Induced Enhancement of Field Effect

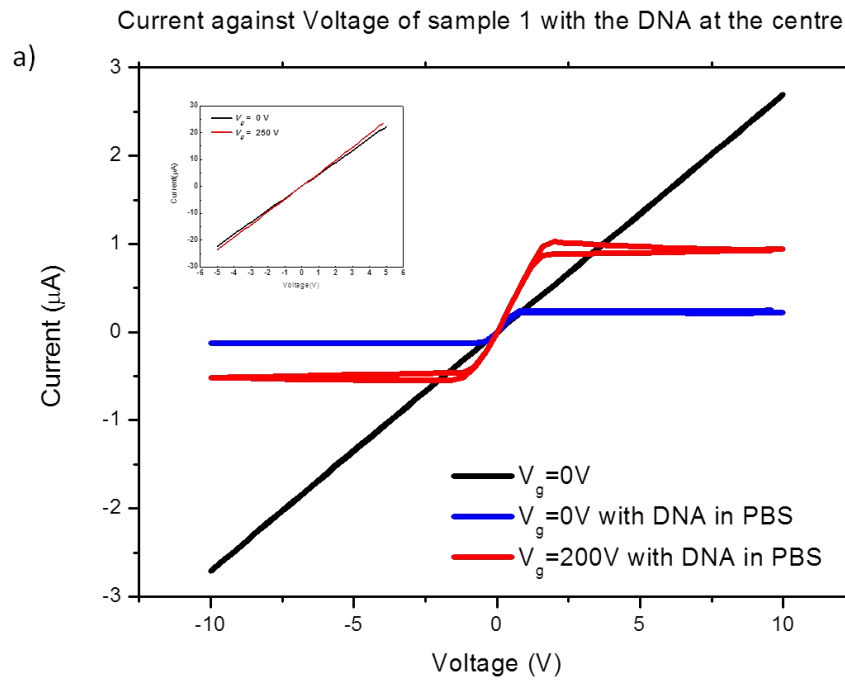
It has been demonstrated by many researchers that the 2DEG transport property can be modulated by back gate field, i.e., a field effect transistor with the 2DEG gas as conducting channel. However, the field effect is relatively quite small as reported in literatures. During this thesis work, it is found that with the presence of water on the surface of the LAO inducing a Schottky junction at the conducting channel, the field effect through back gate is tremendously enhanced.

During the experiment, a droplet of water was placed on top of the sample with the conducting channel fully covered by water. I-V characteristic of such device is shown in Figure 4-7(a), where a FET-like saturation of current occurs. One can see that when a positive bias is applied through the back gate, the saturation current was largely

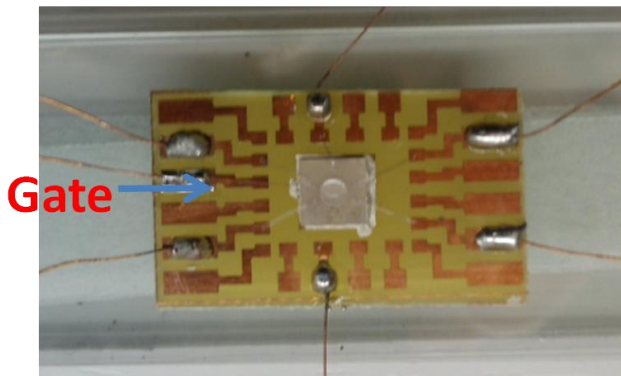


THE HONG KONG POLYTECHNIC UNIVERSITY

increased. From the literature, for example Ref.[7] with the result shown at the top left corner, the resistance of LAO/STO heterointerface can only be slightly affected by the external bias when the LAO surface is not covered by water. This phenomenon can be understood by thinking that the back gate field modulates the current through the 2DEG channel by modifying the charge carrier density; while when water droplet presents on the surface of the 2DEG and a Schottky junction is built up, the current through the conducting channel will be largely affected by the back gate field through modulating the junction thickness and height, and therefore is more sensitive. This may make the 2DEG applicable for real application.



b)



c)

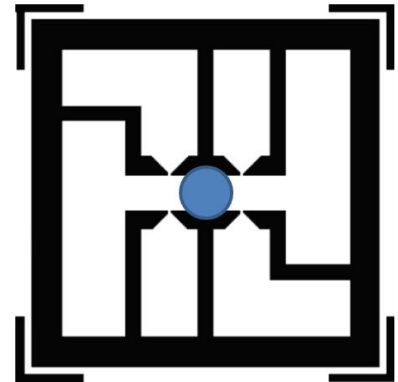


Figure 4-7 a) I -V curves of the LAO/STO interface with/without PBS droplet on top of LAO surface and fully cover the conducting channel, while an external voltage is added by back gate. The I-V curve of the bare sample applied with back gate is shown as the reference; b) the photo of the sensor prototype; c) the pattern used for photolithography. Note: for this testing, there is no observable difference between water, PBS (water with K and Na ions) or PBS with DNA. So, only the data using PBS with DNA is used.

**4.6.2 The 2DEG as DNA Sensor**

To make the 2DEG into a DNA sensor is one of the original ideas in this thesis work, and preliminary results have been obtained even though a reliable model is still not available to interpret the results. Considering the fact that the surface of LAO is very sensitive to polar molecule and the chain of Deoxyribonucleic acid (DNA) contains negative charges [92], it is reasonable to expect that the 2DEG is sensitive to the presence of DNA on top of the LAO/STO surface. In this session, the testing results are presented.

During the sample preparation, LAO thin film was deposited on TiO₂-terminated STO substrate, and the patterned thin film was placed on a PCB. The connections between LAO/STO heterointerface and copper pad on PCB were made by ultrasound wire bonding. The sample was coated by parylene for water-proof purpose (shown in Figure 3-6).

During the experiment, two LAO/STO samples were used, one in the PBS (water with K⁺ and Na⁺ ions) and the other one with PBS and DNA. The I-V characteristics of those samples were measured at different time periods. One can see that, there is a significant difference between the I-V curves for the samples in contact with PBS with and without DNA; with DNA in PBS, clear hysteresis loops appear in the I-V curves. It is believed that the large DNA molecules results in slow movement



THE HONG KONG POLYTECHNIC UNIVERSITY

compared to the water molecules or K^+ and Na^+ ions, and the slow movement may be responsible for the formation of I-V loops. However, a more detailed understanding on the results needs further detailed study.

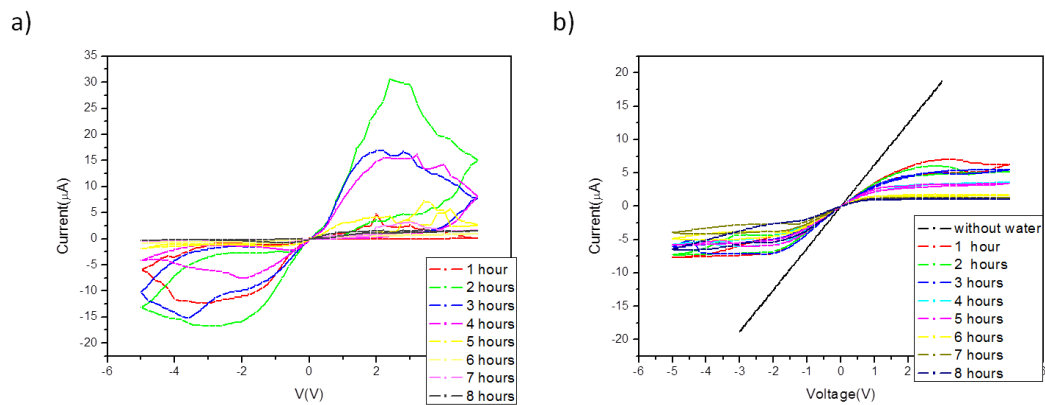


Figure 4-8 I-V curves of sensors contact with (a) PBS with DNA, (b) PBS without DNA.

4.7 Summary

In this Chapter, I have demonstrated potential application of LAO/STO interfacial 2DEG as polar molecule sensor and presented an explanation to the sensing mechanism using a built-up Schottky junction model. These results suggest that this type of sensor may be extended to applications in DNA sensing as well as polar gas molecule sensing if a gas catalytic layer can be coated on the sensor surface. Also, the polar liquid induced saturation current can be highly affected by the external bias.



Chapter 5 Formation of Schottky Junction at LAO/STO Interface with Amorphous STO on LAO

5.1 Introduction

In Chapter 4, the application of LAO/STO interfacial 2DEG as polar molecule sensor has been demonstrated. To explain such a sensing mechanism, a Schottky junction model has been proposed, in which a droplet of water changes the 2DEG into semiconducting, and therefore a metal-semiconductor junction is formed. At the same time, it opens several new questions. One of the questions should be "how can we know the area affected by water changed from metallic to semi-conducting?" Of course, from the result of I-V curve in Chapter 4 (Figures 4-1 and 4-2), the saturated current implies the formation of a Schottky junction. The part of the conducting channel of the 2DEG which exposes to atmosphere (not covered by water) should still be metallic; therefore, the conducting channel affected by water should be changed to semiconducting. It is a reasonable explanation; however, there is still not direct experimental result or any simulation result to proof it, even there are a few experiments related to the junction between semiconductor and 2DEG in LAO/STO system[40, 88]. In this chapter, similar results to the case with water will be demonstrated using formation of a Schottky junction by depositing amorphous-STO (a-STO) on LAO.



5.2 Experimental Detail

LaAlO₃ films were deposited by laser-molecular beam epitaxy (L-MBE) with a KrF excimer laser ($\lambda = 248$ nm) on TiO₂-terminated STO single crystal substrates. Prior to the deposition, the substrate was pre-cleaned by acetone and ethanol to remove any organic remnants on it. During the deposition, the substrate temperature was maintained at 750 °C and about 1×10^{-4} to 3 Pa O₂ pressure. The laser pulse repetition rate is 1Hz. After deposition, the samples were in-situ annealed under 10 mbar of O₂ pressure for 1 hour at a reduced temperature of 550°C and then were cooled down to room temperature in the same ambient. A piece of stainless steel was used as the mask on the centre of sample. A layer of amorphous STO was deposited by the same system at a temperature of 150°C and at about 5×10^{-5} Pa vacuum condition. The laser pulse repetition rate is 10Hz. The samples were cooled down to room temperature in the same ambient.

The interfaces were contacted by aluminum wire using an ultrasonic wire-bonding machine for further transport properties measurements. The structure of the sample is showed in Figure 5-1. Current-voltage (I-V) characteristics were measured using Keithley 2400 source meter with the control of Labview.

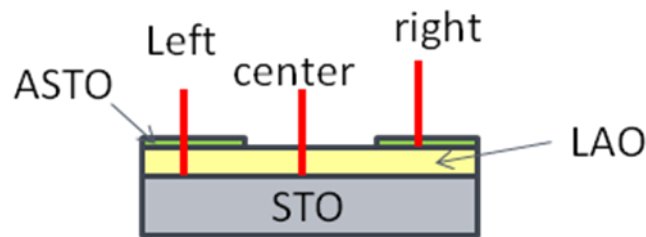


Figure 5-1 Schematic diagram of the sample profile. For the connection between left side and centre, it is a typical connection of 2DEG. For the connection between right side and centre, a junction is formed between the 2DEG and the LAO layer.

5.3 Result and Discussion

5.3.1 Schottky Junction of between the 2DEG and a-STO

In order to understand the Schottky junction formed in the LAO/STO heterointerface 2DEG, a n-type semiconductor a-STO has been grown on LAO gate area to form a junction with the 2DEG, as shown in Figure 5-2 (b). The I-V characteristic of the connection has been measured at the room temperature, as shown in Figure 5-2 (a). From the I-V curve, it can be seen that a diode-like rectifying effect has been formed. This saturation of the current indicates that a metal and n-type semiconductor Schottky junction has been formed between the 2DEG and a-STO. It should be noticed that the direction of saturation induced by the external bias is opposite to a typical metal-n type semiconductor junction; while it is the same case for the Schottky junction mentioned in Chapter 4.

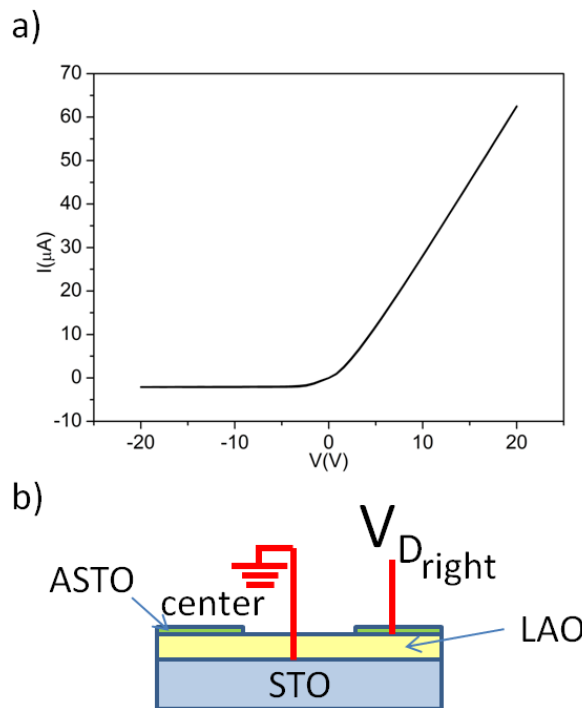


Figure 5-2 (a) I -V curves of the connection between centre of sample and the right side, and (b) schematic diagram illustrating the connection of model. At the centre, the Aluminum wire is connected to the heterointerface by passing through the LAO thin film. For the Aluminum wire at the right side, it doesn't touch to the interface. This can be controlled by wire bonding force.

5.3.2 Effect of Water on a-STO and 2DEG

From the above experiment, it can be understood that a junction can be formed when the 2DEG contact to a-STO or the polar liquid induced semiconducting region. In the following experiment, I try to combine them together and analyze their behavior.

I-V characteristics of the sample with patterned a-STO deposited on LAO/STO were measured at room temperature (shown in Figure 5-3). In Figure 5-3(a), a linear



THE HONG KONG POLYTECHNIC UNIVERSITY

relation of I-V curve shows the ohmic contact for the connection from centre to left side; while the curve corresponding to Figure 5-3(c) shows the similar result as in Chapter 4. For the curve corresponding to Figure 5-3(d), two saturations occur for the positive and negative bias, but with different saturation currents. Considering the flowing direction of electrons, the $13\mu\text{A}$ saturation current should be induced by the junction formed between the 2DEG and a-STO, and the $21\mu\text{A}$ saturation current should be induced by the junction of the 2DEG with semiconducting region affected by water. In Figure 5-3(e), the $23\mu\text{A}$ saturation current is due to the junction formed by the 2DEG with a-STO covered by water. From the above results, it can be understood that the polarity of water can cross the a-STO layer and affect the conducting behavior of the LAO/STO interface.

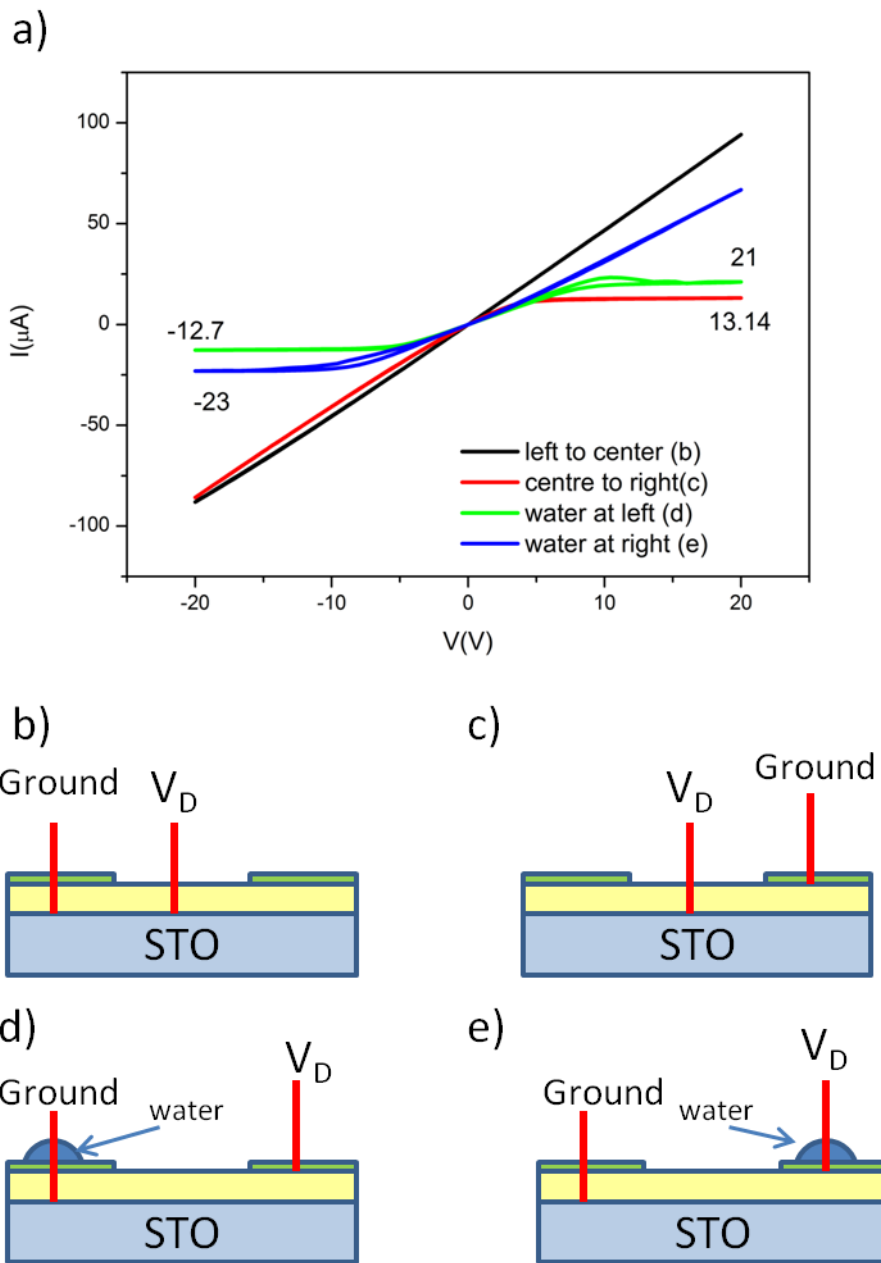


Figure 5-3 (a) I-V curves of the sample under different connections at room temperature, and from (b) to (e) are schematic diagram illustrating the connection models.



5.3.3 Temperature-Dependent I-V Characteristics of the 2DEG/a-STO Schottky Junction

In order to understand the behaviors of the above formed junctions, study of temperature-dependent electric transport properties is important. I-V characteristics of the samples were measured at different temperatures and the results are shown in Figure 5-4. Figure 5-4(a) shows the I-V curves of the connections between centre and right, representing the characteristic of the junction; whereas Figure 5-4(b) shows the I-V curves of the connections between centre and left, representing the characteristic of the 2DEG. The results illustrate a strong temperature dependence of the I-V characteristics across the junction. Some I-V curves of the connections from centre to right measured at different temperatures are further plotted out, as shown in Figure 5-4(c), where two trends can be found.

Firstly, one can see that the saturated current increases when the measuring temperature decreases. From the I-V curves measured at 300 to 140 K, it is apparent that the saturation of the current gradually increases; however, no saturation of current can be observed when temperature is lower than 130 K. This phenomenon may also be explained by the Schottky junction model proposed in Chapter 4. It is worth noting that the carrier density of the 2DEG is much lower compared to a typical metal; a non-negligible local depletion layer in the metallic 2DEG region may be formed near to the junction. When temperature decreases, the carrier density of the 2DEG is nearly



THE HONG KONG POLYTECHNIC UNIVERSITY

unchanged compared to that of semiconductor which decreases exponentially. Therefore, the thickness of depletion layer in the 2DEG region reduces with decreased temperature due to inversely proportional relationship between the thickness of depletion layer and carrier concentration [93]. As a result, at a relatively low temperature, electrons tunnel through the junction more easily and therefore results in an increased saturation current.

Secondly, one can notice that there is a hump in the I-V curve before reaching saturation during voltage sweep, but this does not happen when voltage sweeps back; i.e., a loop-like I-V characteristic is formed. At room temperature, the difference between the values of local maximum and saturation current is very small; therefore, the formed loop is extremely small. However, when temperature is decreased, the difference between the value of local maximum and the value of saturation becomes larger and larger. To explain this interesting phenomenon, a model based on Joule heating is proposed. It is believed that during the I-V measurement, the electrical energy should mainly dissipates at the LAO/STO heterointerface. For a bare LAO/STO sample, the energy dissipates at the heterointerface evenly; however, for the LAO/STO sample with a Schottky junction, most of the energy should be dissipated at the junction when electrons move across it. The dissipated heat energy close to the junction should also increase when the bias voltage increases, and therefore, the area close to the junction will be heated up due to Joule heating. As the thickness of depletion layer is related to the number of carriers of the two sides of the junction, this heating induced temperature increase should cause the increase of depletion layer's thickness of the 2DEG and then further restrict electrons passing through the formed junction. Therefore, the measured



THE HONG KONG POLYTECHNIC UNIVERSITY

current should first rise to a maximum and then decrease. Finally, it reaches an equilibrium state when the Joule heating rate is equal to the rate of heat dissipation, and therefore a stable saturation current is obtained. At room temperature, this effect is not very obvious and even cannot be observed as the current of the system is quite small, so that the energy dissipation is relatively low and the equilibrium is easy to reach. However, when temperature decreases, the junction allows a larger current to go through it first, and therefore, longer time is needed to reach the equilibrium and a larger hump is formed.

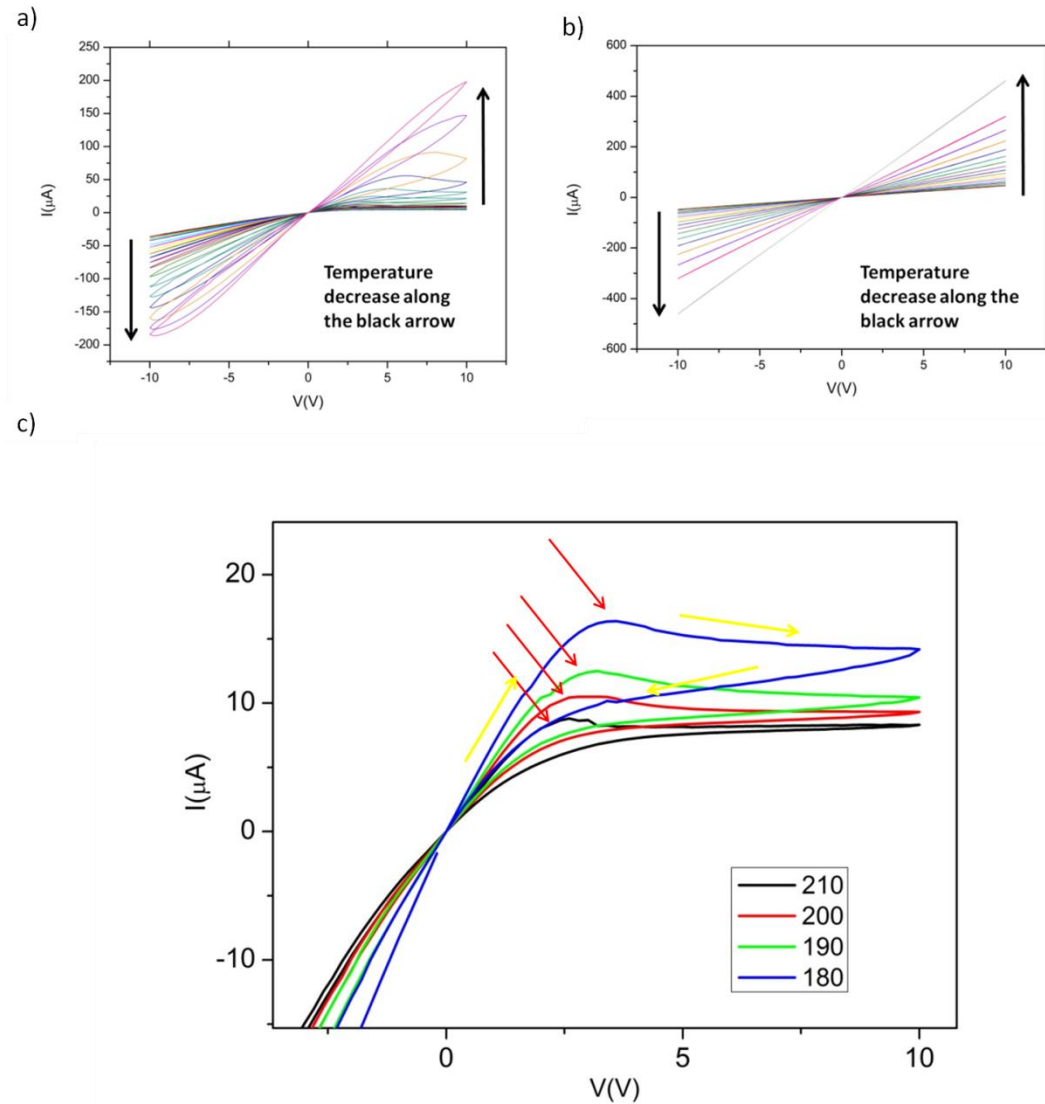


Figure 5-4 I-V curves of the junction at different temperatures from 300K to 120K with an interval of 10K: a) the temperature-dependent I-V curves measured by centre to right; b) the temperature-dependent I-V curves measured by centre to left, (S6101 centre to right with a-STO); c) I-V curves at temperatures from 210K to 180K. The red arrow indicates the current maxima and the yellow arrow indicates the direction of loops.



5.4 Summary

In this chapter, samples with the aim to illustrate the Schottky junction in the LAO/STO 2DEG system were fabricated, where a layer of amorphous STO was deposited on top of the LAO/STO sample. From the I-V measurement result, it can be found that the current is saturated at relatively high bias voltage. The direction of saturation is the same as the saturation caused by polar liquid on top of the LAO/STO (results in Chapter 4). The saturation current and the corresponding voltage are found to increase when the measuring temperature decreases. A hysteresis loop-like I-V characteristic was founded, and the loop area increases as temperature decreases.



Chapter 6 Conclusion and Perspectives

In this thesis work, the 2DEG in LAO/STO heterointerface has been formed by L-MBE growth of LAO film on TiO₂-terminated STO substrate. Sensing phenomenon of this 2DEG to polar liquids has been demonstrated and the sensing mechanism has been proposed. The main discoveries of this thesis work are summarized as following:

- (1) The method of treatment of commercial STO substrate to obtain TiO₂-terminated high-quality STO substrate has been achieved.
- (2) The growth of high-quality LAO/STO heterostructure by Laser-MBE has been achieved. The electric transport properties measurements have proven that the 2DEG has been formed at this heterostructure and the results are similar to the literature reported results.
- (3) It has been demonstrated that this 2DEG is very sensitive to polar liquids such as water.
- (4) A model has been proposed based on the formation of a Schottky junction when water presents at the gate area in the field effect transistor structure with the 2DEG as conducting channel.
- (5) Depositing a-STO on LAO across the FET gate area results in a Schottky junction similar to the case when water presents on the LAO surface.



THE HONG KONG POLYTECHNIC UNIVERSITY

However, there are some limitations that have not been achieved in the thesis work which need further study. For example, the LAO/STO 2DEG is sensitive to polar liquids, making it difficult to sense DNA which is usually dissolved in water. This problem needs to be solved by new approaches such as surface modification of the LAO surface or the liquid dissolving DNAs. Even we proposed the Schottky junction model to interpret the FET-like I-V curve when water presents on the LAO surface, there is still no direct experimental work or theoretical result to prove it. In addition, the selectivity to different polar liquids is not known, since it is difficult to maintain the same amount and position of different liquids on the sensor. Micro-fluidic device utilizing the LAO/STO 2DEG may make it possible to differentiate different polar liquids by the amount of change of the current. These are good topics for future study, and in long term, it could open a new research field of real application of the 2DEG.



References

- [1] J. H. Park, E. Vescovo, H. J. Kim, C. Kwon, R. Ramesh, and T. Venkatesan, "Direct evidence for a half-metallic ferromagnet," *Nature*, vol. 392, 794-796, 1998.
- [2] W. Eerenstein, N. D. Mathur, and J. F. Scott, "Multiferroic and magnetoelectric materials," *Nature*, vol. 442, 759-765, 2006.
- [3] A. Ohtomo and H. Y. Hwang, "A high-mobility electron gas at the LaAlO₃/SrTiO₃ heterointerface," *Nature*, vol. 427, 423-426, 2004.
- [4] A. Brinkman, M. Huijben, M. van Zalk, J. Huijben, U. Zeitler, J. C. Maan, W. G. van der Wiel, G. Rijnders, D. H. A. Blank, and H. Hilgenkamp, "Magnetic effects at the interface between non-magnetic oxides," *Nat Mater*, vol. 6, 493-496, 2007.
- [5] W. Siemons, G. Koster, H. Yamamoto, W. A. Harrison, G. Lucovsky, T. H. Geballe, D. H. A. Blank, and M. R. Beasley, "Origin of charge density at LaAlO₃ on SrTiO₃ heterointerfaces: Possibility of intrinsic doping," *Physical Review Letters*, vol. 98, 2007.
- [6] G. Herranz, M. Basletic, M. Bibes, C. Carretero, E. Tafrá, E. Jacquet, K. Bouzehouane, C. Deranlot, A. Hamzic, J. M. Broto, A. Barthelemy, and A. Fert, "High mobility in LaAlO₃/SrTiO₃ heterostructures: Origin, dimensionality, and perspectives," *Physical Review Letters*, vol. 98, 2007.
- [7] S. Thiel, G. Hammerl, A. Schmehl, C. W. Schneider, and J. Mannhart, "Tunable Quasi-Two-Dimensional Electron Gases in Oxide Heterostructures," *Science*, vol. 313, 1942-1945, 2006.
- [8] L. Li, C. Richter, J. Mannhart, and R. C. Ashoori, "Coexistence of magnetic order and two-dimensional superconductivity at LaAlO₃/SrTiO₃ interfaces," *Nature Physics*, vol. 7, 762-766, 2011.
- [9] N. Reyren, M. Bibes, E. Lesne, J. M. George, C. Deranlot, S. Collin, A. Barthelemy, and H. Jaffres, "Gate-Controlled Spin Injection at LaAlO₃/SrTiO₃ Interfaces," *Physical Review Letters*, vol. 108, 2012.



THE HONG KONG POLYTECHNIC UNIVERSITY

- [10] N. Reyren, S. Thiel, A. D. Caviglia, L. F. Kourkoutis, G. Hammerl, C. Richter, C. W. Schneider, T. Kopp, A.-S. Rüetschi, D. Jaccard, M. Gabay, D. A. Muller, J.-M. Triscone, and J. Mannhart, "Superconducting Interfaces Between Insulating Oxides," *Science*, vol. 317, 1196-1199, 2007.
- [11] C. Cen, S. Thiel, G. Hammerl, C. W. Schneider, K. E. Andersen, C. S. Hellberg, J. Mannhart, and J. Levy, "Nanoscale control of an interfacial metal-insulator transition at room temperature," *Nat. Mater.*, vol. 7, 298-302, 2008.
- [12] C. Cen, S. Thiel, J. Mannhart, and J. Levy, "Oxide Nanoelectronics on Demand," *Science*, vol. 323, 1026-1030, 2009.
- [13] C. W. Bark, P. Sharma, Y. Wang, S. H. Baek, S. Lee, S. Ryu, C. M. Folkman, T. R. Paudel, A. Kumar, S. V. Kalinin, A. Sokolov, E. Y. Tsymlal, M. S. Rzchowski, A. Gruverman, and C. B. Eom, "Switchable Induced Polarization in LaAlO₃/SrTiO₃ Heterostructures," *Nano Letters*, vol. 12, 1765-1771, 2012.
- [14] A. Rastogi and R. C. Budhani, "Solar blind photoconductivity in three-terminal devices of LaAlO₃/SrTiO₃ heterostructures," *Optics Letters*, vol. 37, 317-319, 2012.
- [15] A. Tebano, E. Fabbri, D. Pergolesi, G. Balestrino, and E. Traversa, "Room-Temperature Giant Persistent Photoconductivity in SrTiO₃/LaAlO₃ Heterostructures," *Acs Nano*, vol. 6, 1278-1283, 2012.
- [16] Y. Xie, Y. Hikita, C. Bell, and H. Y. Hwang, "Control of electronic conduction at an oxide heterointerface using surface polar adsorbates," *Nat Commun*, vol. 2, 494, 2011.
- [17] A. Tsukazaki, A. Ohtomo, T. Kita, Y. Ohno, H. Ohno, and M. Kawasaki, "Quantum Hall effect in polar oxide heterostructures," *Science*, vol. 315, 1388-1391, 2007.
- [18] R. Pool, "A Transistor That Works Electron by Electron," *Science*, vol. 249, 629-629, 1990.
- [19] M. Sundaram, S. A. Chalmers, P. F. Hopkins, and A. C. Gossard, "New Quantum Structures," *Science*, vol. 254, 1326-1335, 1991.
- [20] K. Vonklitzing, G. Dorda, and M. Pepper, "New Method for High-



THE HONG KONG POLYTECHNIC UNIVERSITY

- Accuracy Determination of the Fine-Structure Constant Based on Quantized Hall Resistance," *Physical Review Letters*, vol. 45, 494-497, 1980.
- [21] Wikipedia. *2DEG*. Available: http://en.wikipedia.org/wiki/Two_dimensional_electron_gas
- [22] M. Breitschaft, V. Tinkl, N. Pavlenko, S. Paetel, C. Richter, J. R. Kirtley, Y. C. Liao, G. Hammerl, V. Eyert, T. Kopp, and J. Mannhart, "Two-dimensional electron liquid state at LaAlO₃-SrTiO₃ interfaces," *Physical Review B*, vol. 81, 153414, 2010.
- [23] M. Martens, J. Schlegel, P. Vogt, F. Brunner, R. Lossy, J. Wurfl, M. Weyers, and M. Kneissl, "High gain ultraviolet photodetectors based on AlGaIn/GaN heterostructures for optical switching," *Applied Physics Letters*, vol. 98, 2011.
- [24] J. Schalwig, G. Müller, M. Eickhoff, O. Ambacher, and M. Stutzmann, "Gas sensitive GaN/AlGaIn-heterostructures," *Sensors and Actuators B: Chemical*, vol. 87, 425-430, 2002.
- [25] Y. Kawano, T. Uchida, and K. Ishibashi, "Terahertz sensing with a carbon nanotube/two-dimensional electron gas hybrid transistor," *Applied Physics Letters*, vol. 95, 083123-3, 2009.
- [26] A. D. Caviglia, S. Gariglio, N. Reyren, D. Jaccard, T. Schneider, M. Gabay, S. Thiel, G. Hammerl, J. Mannhart, and J. M. Triscone, "Electric field control of the LaAlO₃/SrTiO₃ interface ground state," *Nature*, vol. 456, 624-627, 2008.
- [27] W. J. Son, E. Cho, B. Lee, J. Lee, and S. Han, "Density and spatial distribution of charge carriers in the intrinsic n-type LaAlO₃-SrTiO₃ interface," *Physical Review B*, vol. 79, 2009.
- [28] J. Lee and A. A. Demkov, "Charge origin and localization at the n-type SrTiO₃/LaAlO₃ interface," *Physical Review B*, vol. 78, 193104, 2008.
- [29] R. Pentcheva and W. E. Pickett, "Avoiding the Polarization Catastrophe in LaAlO₃ Overlayers on SrTiO₃(001) through Polar Distortion," *Physical Review Letters*, vol. 102, 2009.
- [30] Z. S. Popović, S. Satpathy, and R. M. Martin, "Origin of the Two-Dimensional Electron Gas Carrier Density at the LaAlO₃ on SrTiO₃



THE HONG KONG POLYTECHNIC UNIVERSITY

- Interface," *Physical Review Letters*, vol. 101, 256801, 2008.
- [31] M. Salluzzo, J. C. Cezar, N. B. Brookes, V. Bisogni, G. M. Luca, C. Richter, S. Thiel, J. Mannhart, M. Huijben, A. Brinkman, G. Rijnders, and G. Ghiringhelli, "Orbital Reconstruction and the Two-Dimensional Electron Gas at the LaAlO₃/SrTiO₃ Interface," *Physical Review Letters*, vol. 102, 2009.
- [32] A. D. Caviglia, M. Gabay, S. Gariglio, N. Reyren, C. Cancellieri, and J. M. Triscone, "Tunable Rashba Spin-Orbit Interaction at Oxide Interfaces," *Physical Review Letters*, vol. 104, 126803, 2010.
- [33] O. Copie, V. Garcia, C. Bodefeld, C. Carretero, M. Bibes, G. Herranz, E. Jacquet, J. L. Maurice, B. Vinter, S. Fusil, K. Bouzehouane, H. Jaffres, and A. Barthelémy, "Towards Two-Dimensional Metallic Behavior at LaAlO₃/SrTiO₃ Interfaces," *Physical Review Letters*, vol. 102, 2009.
- [34] S. Okamoto, A. J. Millis, and N. A. Spaldin, "Lattice relaxation in oxide heterostructures: LaTiO₃/SrTiO₃ superlattices," *Physical Review Letters*, vol. 97, 2006.
- [35] J. Mannhart, D. H. A. Blank, H. Y. Hwang, A. J. Millis, and J. M. Triscone, "Two-Dimensional Electron Gases at Oxide Interfaces," *Mrs Bulletin*, vol. 33, 1027-1034, 2008.
- [36] S. Okamoto and A. J. Millis, "Electronic reconstruction at an interface between a Mott insulator and a band insulator," *Nature*, vol. 428, 630-633, 2004.
- [37] M. Ben Shalom, M. Sachs, D. Rakhmilevitch, A. Palevski, and Y. Dagan, "Tuning Spin-Orbit Coupling and Superconductivity at the SrTiO₃/LaAlO₃ Interface: A Magnetotransport Study," *Physical Review Letters*, vol. 104, 126802, 2010.
- [38] A. D. Caviglia, S. Gariglio, C. Cancellieri, B. Sacépé, A. Fête, N. Reyren, M. Gabay, A. F. Morpurgo, and J. M. Triscone, "Two-Dimensional Quantum Oscillations of the Conductance at LaAlO₃/SrTiO₃ Interfaces," *Physical Review Letters*, vol. 105, 236802, 2010.
- [39] G. Singh-Bhalla, C. Bell, J. Ravichandran, W. Siemons, Y. Hikita, S. Salahuddin, A. F. Hebard, H. Y. Hwang, and R. Ramesh, "Built-in and induced polarization across LaAlO₃/SrTiO₃ heterojunctions," *Nat Phys*,



THE HONG KONG POLYTECHNIC UNIVERSITY

- vol. 7, 80-86, 2011.
- [40] R. Jany, M. Breitschaft, G. Hammerl, A. Horsche, C. Richter, S. Paetel, J. Mannhart, N. Stucki, N. Reyren, S. Gariglio, P. Zubko, A. D. Caviglia, and J. M. Triscone, "Diodes with breakdown voltages enhanced by the metal-insulator transition of LaAlO_3 -- SrTiO_3 interfaces," *Applied Physics Letters*, vol. 96, 183504-3, 2010.
- [41] J. G. Bednorz and K. A. Muller, "Possible High-Tc Superconductivity in the Ba-La-Cu-O System," *Zeitschrift Fur Physik B-Condensed Matter*, vol. 64, 189-193, 1986.
- [42] G. A. Baraff, J. A. Appelbaum, and D. R. Hamann, "Self-Consistent Calculation of the Electronic Structure at an Abrupt GaAs-Ge Interface," *Physical Review Letters*, vol. 38, 237-240, 1977.
- [43] H. Y. Hwang, "Tuning Interface States," *Science*, vol. 313, 1895-1896, 2006.
- [44] M. Kawasaki, K. Takahashi, T. Maeda, R. Tsuchiya, M. Shinohara, O. Ishiyama, T. Yonezawa, M. Yoshimoto, and H. Koinuma, "Atomic Control of the SrTiO_3 Crystal Surface," *Science*, vol. 266, 1540-1542, 1994.
- [45] J. E. Kleibeuker, G. Koster, W. Siemons, D. Dubbink, B. Kuiper, J. L. Blok, C.-H. Yang, J. Ravichandran, R. Ramesh, J. E. ten Elshof, D. H. A. Blank, and G. Rijnders, "Atomically Defined Rare-Earth Scandate Crystal Surfaces," *Advanced Functional Materials*, vol. 20, 3490-3496, 2010.
- [46] G. Koster, B. L. Kropman, G. J. H. M. Rijnders, D. H. A. Blank, and H. Rogalla, "Quasi-ideal strontium titanate crystal surfaces through formation of strontium hydroxide," *Applied Physics Letters*, vol. 73, 2920-2922, 1998.
- [47] T. Ohnishi, K. Shibuya, M. Lippmaa, D. Kobayashi, H. Kumigashira, M. Oshima, and H. Koinuma, "Preparation of thermally stable TiO_2 -terminated $\text{SrTiO}_3(100)$ substrate surfaces," *Applied Physics Letters*, vol. 85, 272-274, 2004.
- [48] D. Kobayashi, H. Kumigashira, M. Oshima, T. Ohnishi, M. Lippmaa, K. Ono, M. Kawasaki, and H. Koinuma, "High-resolution synchrotron-radiation photoemission characterization for atomically-controlled $\text{SrTiO}_3(001)$ substrate surfaces subjected to various surface treatments,"



THE HONG KONG POLYTECHNIC UNIVERSITY

- Journal of Applied Physics*, vol. 96, 7183-7188, 2004.
- [49] Y. Z. Chen and N. Pryds, "Imposed quasi-layer-by-layer homoepitaxial growth of SrTiO₃ films by large area pulsed laser deposition," *Thin Solid Films*, vol. 519, 6330-6333, 2011.
- [50] M. Kareev, S. Prosandeev, J. Liu, C. Gan, A. Kareev, J. W. Freeland, M. Xiao, and J. Chakhalian, "Atomic control and characterization of surface defect states of TiO₂ terminated SrTiO₃ single crystals," *Applied Physics Letters*, vol. 93, 061909-3, 2008.
- [51] J. Zhang, D. Dou, T. Merz, J. Chakhalian, M. Kareev, J. Liu, and L. J. Brillson, "Depth-resolved subsurface defects in chemically etched SrTiO₃," *Applied Physics Letters*, vol. 94, 092904-3, 2009.
- [52] J. T. Cheung, I. Gergis, M. James, and R. E. DeWames, "Reproducible growth of high quality YBa₂Cu₃O_{7-x} film on (100) MgO with a SrTiO₃ buffer layer by pulsed laser deposition," *Applied Physics Letters*, vol. 60, 3180-3182, 1992.
- [53] R. D. Vispute, R. Chowdhury, P. Tiwari, and J. Narayan, "Pulsed laser deposition and characterization of epitaxial Cu/TiN/Si(100) heterostructures," *Applied Physics Letters*, vol. 65, 2565-2567, 1994.
- [54] R. Ramesh, K. Luther, B. Wilkens, D. L. Hart, E. Wang, J. M. Tarascon, A. Inam, X. D. Wu, and T. Venkatesan, "Epitaxial growth of ferroelectric bismuth titanate thin films by pulsed laser deposition," *Applied Physics Letters*, vol. 57, 1505-1507, 1990.
- [55] N.-J. Seong, S.-G. Yoon, Y.-H. Jo, M.-H. Jung, C.-R. Cho, J.-M. Yang, D.-J. Park, J.-W. Lee, and J.-Y. Lee, "Intrinsic ferromagnetic properties of Ti_{0.94}Fe_{0.06}O₂/Ti_{0.94}Mn_{0.06}O₂ superlattice films for dilute magnetic semiconductor applications," *Applied Physics Letters*, vol. 89, 162109-3, 2006.
- [56] M. Kanai and T. Kawai, "Superconductivity of (Ba,Sr,Ca)CuO₂ Artificial Lattices," *Physica C: Superconductivity*, vol. 235-240, Part 1, 174-177, 1994.
- [57] S. P. Thiel, "Study of Interface Properties in LaAlO₃/SrTiO₃ Heterostructures," Doctoral, der mathematisch-naturwissenschaftlichen Fakultät, der Universität Augsburg, 2009.



THE HONG KONG POLYTECHNIC UNIVERSITY

- [58] F. C. Frank and J. H. van der Merwe, "One-Dimensional Dislocations. I. Static Theory," *Proc. Roy. Soc. London A*, vol. 198, 205, 1949.
- [59] M. Volmer and A. Weber, "Nuclei formation in supersaturated states," *Z. phys. Chem.*, vol. 119, 277, 1926.
- [60] I. N. Stranski and Krastanov, "Theory of orientation separation of ionic crystals," *Acad. Wiss. Math.-Naturw. Klasse Iib*, vol. 146, 797, 1938.
- [61] T. Ohnishi, K. Shibuya, T. Yamamoto, and M. Lippmaa, "Defects and transport in complex oxide thin films," *Journal of Applied Physics*, vol. 103, 103703-6, 2008.
- [62] J. D. Ferguson, G. Arikian, D. S. Dale, A. R. Woll, and J. D. Brock, "Measurements of Surface Diffusivity and Coarsening during Pulsed Laser Deposition," *Physical Review Letters*, vol. 103, 256103, 2009.
- [63] A. Ohtomo and H. Y. Hwang, "Growth mode control of the free carrier density in SrTiO₃ films," *Journal of Applied Physics*, vol. 102, 083704-6, 2007.
- [64] W. Braun, *Applied RHEED: Reflection High-Energy Electron Diffraction During Crystal Growth*. Berlin: Springer, 1999.
- [65] L. laboratory. *Reflection High-Energy Electron Diffraction*. Available: <http://lippmaa.issp.u-tokyo.ac.jp/rheed/>
- [66] Wikipedia. *Atomic force microscopy*. Available: http://en.wikipedia.org/wiki/Atomic_force_microscope
- [67] A. Kalabukhov, R. Gunnarsson, J. Borjesson, E. Olsson, T. Claesson, and D. Winkler, "Effect of oxygen vacancies in the SrTiO₃ substrate on the electrical properties of the LaAlO₃/SrTiO₃ interface," *Physical Review B*, vol. 75, 121404, 2007.
- [68] Wikipedia. *Parylene*. Available: <http://en.wikipedia.org/wiki/Parylene>
- [69] J. B. Fortin and T. M. Lu, "Mass spectrometry study during the vapor deposition of poly-para-xylylene thin films," *Journal of Vacuum Science & Technology A: Vacuum, Surfaces, and Films*, vol. 18, 2459-2465, 2000.
- [70] L. J. Van Der PAUW, "A METHOD OF MEASURING SPECIFIC RESISTIVITY AND HALL EFFECT OF DISCS OF ARBITRARY SHAPE," *Philips Research Reports*, vol. 13, 1-9, 1958.
- [71] Wikipedia. *Van Der Pauw method*. Available:



THE HONG KONG POLYTECHNIC UNIVERSITY

http://en.wikipedia.org/wiki/Van_der_Pauw_method

- [72] Wikipedia. *Hall effect*. Available: http://en.wikipedia.org/wiki/Hall_effect
- [73] Y. Wakabayashi, Y. Yamasaki, C. Bell, Y. Hikita, H. Y. Hwang, and T. Kimura, "Growth Temperature Dependence of the LaAlO₃/SrTiO₃ Interfacial Structure," *International Conference on Frustration in Condensed Matter (IcfcM)*, vol. 320, 2011.
- [74] X. Wang, J. Q. Chen, A. R. Barman, S. Dhar, Q. H. Xu, T. Venkatesan, and Ariando, "Static and ultrafast dynamics of defects of SrTiO₃ in LaAlO₃/SrTiO₃ heterostructures," *Applied Physics Letters*, vol. 98, 2011.
- [75] J. E. Boschker, C. Folkman, C. W. Bark, A. F. Monsen, E. Folven, J. K. Grepstad, E. Wahlstrom, C. B. Eom, and T. Tybell, "Structural coupling across the LaAlO₃/SrTiO₃ interface: High-resolution x-ray diffraction study," *Physical Review B*, vol. 84, 2011.
- [76] H. Chen, A. M. Kolpak, and S. Ismail-Beigi, "Electronic and Magnetic Properties of SrTiO₃/LaAlO₃ Interfaces from First Principles," *Advanced Materials*, vol. 22, 2881-2899, 2010.
- [77] R. Arras, V. G. Ruiz, W. E. Pickett, and R. Pentcheva, "Tuning the two-dimensional electron gas at the LaAlO₃/SrTiO₃(001) interface by metallic contacts," *Physical Review B*, vol. 85, 125404, 2012.
- [78] C. Cazorla and M. Stengel, "First-principles modeling of Pt/LaAlO₃/SrTiO₃ capacitors under an external bias potential," *Physical Review B*, vol. 85, 2012.
- [79] W. J. Son, E. Cho, J. Lee, and S. Han, "Hydrogen adsorption and carrier generation in LaAlO₃-SrTiO₃ heterointerfaces: a first-principles study," *Journal of Physics-Condensed Matter*, vol. 22, 2010.
- [80] S. A. Pauli, S. J. Leake, B. Delley, M. Björck, C. W. Schneider, C. M. Schlepütz, D. Martoccia, S. Paetel, J. Mannhart, and P. R. Willmott, "Evolution of the Interfacial Structure of LaAlO₃ on SrTiO₃," *Physical Review Letters*, vol. 106, 036101, 2011.
- [81] C. W. Bark, D. A. Felker, Y. Wang, Y. Zhang, H. W. Jang, C. M. Folkman, J. W. Park, S. H. Baek, H. Zhou, D. D. Fong, X. Q. Pan, E. Y. Tsymbal, M. S. Rzchowski, and C. B. Eoma, "Tailoring a two-dimensional electron gas at the LaAlO₃/SrTiO₃ (001) interface by epitaxial strain," *PNAS*, vol. 108,



THE HONG KONG POLYTECHNIC UNIVERSITY

- 4720-4724, 2011.
- [82] C. Cancellieri, D. Fontaine, S. Gariglio, N. Reyren, A. D. Caviglia, A. Fête, S. J. Leake, S. A. Pauli, P. R. Willmott, M. Stengel, P. Ghosez, and J. M. Triscone, "Electrostriction at the $\text{LaAlO}_3/\text{SrTiO}_3$ Interface," *Physical Review Letters*, vol. 107, 056102, 2011.
- [83] F. Bi, D. F. Bogorin, C. Cen, C. W. Bark, J.-W. Park, C.-B. Eom, and J. Levy, "'Water-cycle' mechanism for writing and erasing nanostructures at the $\text{LaAlO}_3/\text{SrTiO}_3$ interface," *Applied Physics Letters*, vol. 97, 173110-3, 2010.
- [84] Y. Xie, C. Bell, T. Yajima, Y. Hikita, and H. Y. Hwang, "Charge Writing at the $\text{LaAlO}_3/\text{SrTiO}_3$ Surface," *Nano Letters*, vol. 10, 2588-2591, 2010.
- [85] Y. Xie, C. Bell, Y. Hikita, and H. Y. Hwang, "Tuning the Electron Gas at an Oxide Heterointerface via Free Surface Charges," *Advanced Materials*, vol. 23, 1744-1747, 2011.
- [86] R. Pentcheva, M. Huijben, K. Otte, W. E. Pickett, J. E. Kleibeuker, J. Huijben, H. Boschker, D. Kockmann, W. Siemons, G. Koster, H. J. W. Zandvliet, G. Rijnders, D. H. A. Blank, H. Hilgenkamp, and A. Brinkman, "Parallel Electron-Hole Bilayer Conductivity from Electronic Interface Reconstruction," *Physical Review Letters*, vol. 104, 166804, 2010.
- [87] D. F. Bogorin, C. W. Bark, H. W. Jang, C. Cen, C. M. Folkman, C. B. Eom, and J. Levy, "Nanoscale rectification at the $\text{LaAlO}_3/\text{SrTiO}_3$ interface," *Applied Physics Letters*, vol. 97, 2010.
- [88] W. M. Lu, X. Wang, Z. Q. Liu, S. Dhar, A. Annadi, K. Gopinadhan, A. R. Barman, H. B. Su, T. Venkatesan, and Ariando, "Metal-insulator transition at a depleted $\text{LaAlO}_3/\text{SrTiO}_3$ interface: Evidence for charge transfer induced by SrTiO_3 phase transitions," *Applied Physics Letters*, vol. 99, 2011.
- [89] Gorgia. *PHD thesis*. Available: http://gorgia.no-ip.com/phd/html/thesis/phd_html/node3.html
- [90] CliveTEC_Electronic_resources. *Diodes*. Available: <http://clivetec.0catch.com/Diodes.html>
- [91] T. Susaki, A. Makishima, and H. Hosono, "Work function engineering via $\text{LaAlO}_3/\text{SrTiO}_3$ polar interfaces," *Physical Review B*, vol. 84, 2011.



THE HONG KONG POLYTECHNIC UNIVERSITY

- [92] Wikipedia. *DNA*. Available: <http://en.wikipedia.org/wiki/DNA>
- [93] S. O. Kasap, *Principles of Electrical Engineering Materials and Devices*: IRWIN, 1996.